A model-based examination of multivariate physical modes in the Gulf of Alaska

A. J. Hermann[1,2], C. Ladd[2], W. Cheng[1], E. N. Curchitser[3], K. Hedstrom[4]

1. Joint Institute for the Study of the Atmosphere and Ocean, University of Washington, Seattle, WA 98195, U.S.A. E-mail: albert.j.hermann@noaa.gov

2. Ocean Environment Research Division, NOAA/PMEL, Seattle, WA 98195, U.S.A.

3. Institute of Marine and Coastal Sciences, Rutgers University, New Brunswick, NJ 08901, U.S.A.

4. Arctic Region Supercomputing Center, Fairbanks, AK 99775, U.S.A.

Corresponding author address:

Albert J. Hermann

Pacific Marine Environmental Laboratory

7600 Sand Point Way NE

Seattle, WA 98115 U.S.A.

Email: albert.j.hermann@noaa.gov

Phone: 206-526-6495

Fax: 206-526-6485

Keywords: USA, Alaska, Gulf of Alaska, modelling

ABSTRACT

We use multivariate output from a hydrodynamic model of the Gulf of Alaska (GOA) to explore the covariance among its physical state and air/sea fluxes. We attempt to summarize this coupled variability using a limited set of patterns, and examine their correlation to three large-scale climate indices relevant to the Northeast Pacific. This analysis is focused on perturbations from monthly climatology of the following attributes of the GOA: sea surface temperature, sea surface height, mixed layer depth, sea surface salinity, latent heat flux, sensible heat flux, shortwave irradiance, net long wave irradiance, currents at 40m depth, and wind stress. We identified two multivariate modes, both substantially correlated with the Pacific Decadal Oscillation (PDO) and Multivariate El Nino (MEI) indices on interannual timescales, which together account for ~30% of the total normalized variance of the perturbation time series. These two modes indicate the following covarying events during periods of positive PDO/MEI: 1) anomalously warm, wet and windy conditions (typically in winter), with elevated coastal SSH, followed 2-5 months later by 2) reduced cloud cover, with emerging shelf-break eddies. Similar modes are found when the analysis is performed separately on the eastern and western GOA; in general, modal amplitudes appear stronger in the western GOA.

1. Introduction

1.1. Overview of the GOA

The coastal Gulf of Alaska (GOA) supports major marine resources, and is governed by unique physical dynamics which include: substantial tidal mixing; strong eastern and western boundary currents; seasonal downwelling circulation; along-canyon transport; intermittent cross-shelf transport by eddies; upwelling via wind stress curl (Stabeno et al. 2004, Stabeno et al. this issue-a,b). Janout et al. (2010) described anomalous ocean cooling events in the GOA during 2006-2008, their formation by winter air-sea heat flux, and their modulation by runoff, winds, and other factors. Janout et al. (2013) elaborated on these findings with a climatological average heat budget at the northern head of the GOA, based on oceanographic and atmospheric data and reanalyses. They emphasized the importance of the Alaska Coastal Current (ACC) in replenishing the oceanic heat lost to the atmosphere each year in the GOA, and concluded that nearshore regions experience greater wintertime heat loss than the middle and outer shelves.

1.2 Goals of this analysis

Here we explore the physical dynamics of the GOA, including air-sea fluxes, as part of the Gulf of Alaska Integrated Ecosystem Program (GOAIERP). The GOAIERP is a vertically integrated field and modeling study of the physics, lower trophic level and fish dynamics of the GOA. The overarching goal of the program is to identify the primary physical and biological factors contributing to successful recruitment of five commercially and ecologically important groundfish species (Pacific cod, pollock, Pacific ocean perch, sablefish, and arrowtooth flounder). A primary hypothesis is that recruitment is largely determined by interannually-varying barriers to survival during early life stages - specifically, the “gauntlet” that larvae must overcome to reach juvenile nursery grounds. To help address this issue, we consider whether the physical dynamics of the GOA as a whole, or subregions thereof, can be broadly classified into a small number of spatiotemporal modes with strong interannual variance. We further consider whether such modes correlate to larger-scale patterns of the wider North Pacific.

To this end, using multivariate EOF analysis, we have examined a suite of physical variables from regional circulation model output (~10 km horizontal resolution), including air-sea flux of heat and momentum based on the atmospheric forcing fields and the evolving oceanic state. We examine the covariance structure of these fields, in order to summarize the combined physical state of the GOA using a limited set of spatial/temporal patterns. We compare the temporal evolution of those structures with the temporal amplitude of three large-scale atmospheric/oceanic patterns ("climate indices") that are generally considered to impact the GOA. Ultimately this may help GOA researchers to interpret the biological variability of the GOA, as the ecosystem experiences these coupled multivariate physical phenomena.

The large-scale patterns chosen for comparison were the Multivariate ENSO Index (MEI) (Wolter and Timlin 1993, 1998), the Pacific Decadal Oscillation (PDO) (Mantua et al. 1997) and the North Pacific Gyre Oscillation (NPGO) (DiLorenzo et al. 2008). The spatial pattern of the PDO in particular has strong amplitude along the coastal Northeast Pacific (Mantua et al. 1997), and has been cited in numerous biological studies. In the GOA itself, many studies have suggested a link between the interannual variability of Sitka eddies and ENSO. Downwelling coastal Kelvin waves excited by ENSO (Melsom et al., 1999; Murray et al., 2001) as well as atmospheric teleconnections with the tropics (Melsom et al., 2003; Okkonen et al., 2001) contribute to interannual mesoscale variability in the eastern GOA (Hermann et al., 2009). The NPGO represents a simultaneous (positively correlated) variation of the subtropical gyre (which includes the California Current system) and the subpolar gyre (which includes the Alaska Current) of the Northeast Pacific. It has been shown to correlate with low-frequency fluctuations in salinity and nutrients at Line P (DiLorenzo et al., 2009), which is located southeast ("upstream") of the GOA (see Fig. 1).

Our analysis is focused on perturbations from monthly climatology of the following attributes of the GOA: sea surface temperature, sea surface height, mixed layer depth, sea surface salinity, latent heat flux, sensible heat flux, shortwave irradiance, net long wave irradiance, currents at 40m depth, and wind stress (see Table 1). Some of these variables are available directly from observations for limited time periods and location, or derivable from observations using bulk flux algorithms, as in Janout et al. (2013). However, our multivariate analysis requires a self-consistent, uniformly gridded set of atmospheric and oceanic properties at scales finer than those typically available from global ocean reanalyses, and ideally spanning multiple decades for all variables. Lacking ready access to a fine-scale, multidecadal, data-assimilating, two-way coupled air-sea simulation for the GOA, we instead utilized output from a regional model with ~10 km horizontal resolution spanning the GOA, driven by a global atmospheric reanalysis. We recognize that this approach excludes both direct feedback of the ocean on the atmosphere, and likewise excludes mesoscale atmospheric features such as gap winds which have been shown to impact GOA circulation (Ladd and Cheng, this issue; Ladd et al., this issue). Despite these shortcomings, our chosen method benefits from a consistent oceanic hindcast at sufficiently fine scale to resolve most of the energetic features of the GOA, including: the Alaska Current/Alaskan Stream system, the Alaskan Coastal Current, and the formation and detachment of shelf-break eddies at ~200 km scale (Stabeno et al., 2004). Impacts of the specific model configuration on our results are discussed further in Section 4.

2. Methods

2.1 The hydrodynamic model

We performed the multivariate analysis on output from an existing regional model spanning the GOA during 1970-2005 (Fig. 1). This model is an implementation of the Regional Ocean Modeling System (ROMS) for the Northeast Pacific (NEP-5) described by Danielson et al. (2012). ROMS is a sigma-coordinate model with curvilinear horizontal coordinates; a description of basic features and implementation can be found in Haidvogel et al. (2008) and Shchepetkin and McWilliams (2005). The NEP-5 grid has approximately 10 km horizontal resolution, with 60 vertical levels. Fine-scale bathymetry is based on ETOPO5 and supplementary datasets as described in Danielson et al. (2012); smoothing of that bathymetry was utilized for numerical stability. Any regions shallower than 10m were set to be 10m deep. Mixing is based on the algorithms of Large et al. (1994). Both ice (Budgell, 2005) and tidal dynamics are included in this model; the explicit inclusion of tidal flows allows tidally-generated mixing and tidal residual flows to develop. Freshwater runoff was applied by freshening of the salinity field within a few gridpoints of the coastline, using the climatology of Dai et al. (2009). Bulk forcing, based on algorithms of Large and Yeager (2009), were used to relate winds, air temperature, relative humidity, and downward shortwave and longwave irradiance to surface stress and the net transfers of sensible heat, latent heat, net shortwave and net longwave irradiance through the sea surface. The Common Ocean Reference Experiment reanalysis (CORE; Large and Yeager, 2008) was utilized for atmospheric forcing during the hindcast years. Use of this product suggests that we will resolve large-scale interannual variability, as the ocean model is driven by interannually varying observed winds and temperatures. We will incompletely resolve the details of mesoscale eddies, as we do not explicitly assimilate ocean data at those scales; however, we can reasonably expect to capture the statistics of these eddies between years, as they are influenced by the larger-scale fields.

Extensive comparisons of NEP-5 results with data for the Bering Sea are described in Curchitser et al. (2010), Danielson et al. (2011) and (with a slightly modified version) in Hermann et al. (2013, 2015). These comparisons exhibited good agreement with ice cover, tidal velocities and subsurface temperature data (Danielson et al. 2011), as well as multiannual moored temperature and salinity data (Hermann et al. 2013) and broad-scale hydrographic surveys (Hermann et al. 2015). Comparisons of a previous version of this model (NEP-4) with data in the Gulf of Alaska are described in Parada et al. (this issue). This comparison demonstrated good correspondence of a model-derived climatology of velocities at 40m depth with an equivalent climatology derived from drogued drifter data (Stabeno et al., this issue-a).

Ocean dynamics relevant to the present study include the formation of mesoscale eddies at the shelf break, and their subsequent migration offshore (e.g. Ladd et al., 2007). One measure of eddy strength and frequency is eddy kinetic energy (EKE); as in Ladd (2007), we define this as one-half the average squared surface geostrophic velocity anomaly (where that anomaly is calculated relative to the long-term mean value at each location). Coyle et al. (2014) reported how the EKE field derived from the NEP-5 model over a 5-year period compared to that derived from altimeter data. They found that broad features of the model EKE climatology were similar to data, but at reduced amplitude. The modeled EKE time series exhibited only modest correlation with the observations for the period 2001-2005, when comparing spatial averages over three localized (~100x100 km) sites of observed EKE maxima. In the present study we compare modeled with observed EKE after spatially averaging over a larger domain, 139W-

136W and 56.5N-58N (~200x200 km; Fig. 1). The altimeter data were obtained as described in Ladd (2007). We exclude all areas shallower than 200m, and utilize the full overlapping period of NEP-5 with altimeter data (1993-2005). The chosen domain, located just offshore of Sitka Island, spans a site where GOA eddies frequently form and detach, is large enough to accommodate a single shelf-break eddy at their typical 200-km diameter (Ladd et al., 2007), and allows for slight differences in the formation site between the model and data. The resulting EKE time series, as well as the raw perturbation SSH from the model and data, are used to assess the ability of NEP-5 to capture the formation and detachment of shelf-break eddies in the GOA, in particular during the 1997-1998 El Nino.

2.2 The multivariate EOF analysis

For the statistical analysis of model output, we utilized the method of Coupled Principal Components Analysis (Bretherton et al., 1992). Application of this method to biophysical model output for the Bering Sea has been described in Hermann et al. (2013). Essentially this constructs EOFs from a collection of multivariate time series at the same gridded locations; hence it is a hybrid of univariate EOFs and multivariate Principal Component Analysis. Typical biological use of Principal Components looks for coupled modes of variability in multivariate samples (these may be time series or just scattered samples in space and time), while the typical physical use of Empirical Orthogonal Functions (EOFS) looks for spatial structure of a *single* variable. Here, we use *multivariate* EOFs (space/time/variable) to extract coupled modes that vary through time. Note that the spatial patterns may differ among the different variables. For example, we may look for modes which simultaneously entail a rise in near-coastal SSH with a temporally correlated (but spatially distinct) rise in SST. In each case we normalize the time series (divide by a standard deviation) prior to the analysis, separately using each variable's standard deviation calculated over all space and time. As a result, all variables are unit-less and contribute equally to the analysis. Use of the spatially averaged standard deviations ensures that each variable retains its spatially-modulated time variability, e.g. a stronger signal along the coast than in the deep basin. In the EOF calculation, spatial patterns for each variable are calculated using these normalized time series; the resulting patterns are subsequently multiplied back by the appropriate standard deviation to recover the original units.

Mathematically, the procedure operates as follows:

Consider a collection of L variables $(V(l), l=1..L)$ at N discrete spatial locations $(x_k, k=1..N)$ for which we have monthly mean values over P years $(t_{tyr,mo}, yr=1..P, mo=1..12)$

1) Calculate the climatological monthly values from the original series for each variable $V(l,x,t)$ at each location over P years:

$$V_{mo}(l,x) = \sum_{yr=1}^{P} V\left(l,x,t_{mo,yr}\right)/P$$

2) Subtract the climatological means to obtain the monthly anomalies for each variable with zero mean

$$Vpert\left(l,x,t_{mo,yr}\right) = V\left(l,x,t_{mo,yr}\right) - V_{mo}(l,x)$$

3) Normalize by the standard deviation of the monthly anomalies for each variable, where the variance is calculated over all space and time:

$$\langle Vpert(l)\rangle = \sum_{yr=1}^{P}\sum_{mo=1}^{12}\sum_{k=1}^{N}\left(Vpert\left(l,x_k,t_{yr,mo}\right)\right)^2/(12\,PN)$$

$$Vnorm(l,x,t) = Vpert(l,x,t)/\langle Vpert(l)\rangle^{1/2}$$

4) Calculate the covariance matrix using the normalized anomalies $Vnorm(l,x,t)$. There are now LN time series, each of length $12P$

5) Derive the EOFs (spatial modes for each of the variables and corresponding time series) from the covariance matrix. This is a reconstruction of the original series using orthogonal functions of space/variable (l,x) and time (t) :

$$Vpert(l,x,t) = (X1(l,x)T1(t) + X2(l,x)T2(t) + \cdots)$$

6) Multiply the resulting EOFs by the standard deviation to recover the original units of each variable:

$$V(l,x,t) = \langle Vpert(l) \rangle^{1/2} (X1(l,x)T1(t) + X2(l,x)T2(t) + \cdots)$$

The multivariate spatial modes X are then plotted so as to highlight the amplitude relative to the standard deviation of each variable. Finally, the amplitude time series T for each mode are compared with large-scale indices of the Northeast Pacific: the Multivariate ENSO Index (MEI) (Wolter and Timlin 1993, 1998; http://www.esrl.noaa.gov/psd/enso/mei/), the Pacific Decadal Oscillation (PDO) (Mantua et al. 1997; http://jisao.washington.edu/pdo/) and the North Pacific Gyre Oscillation (NPGO) (DiLorenzo et al. 2008; http://www.o3d.org/npgo/). It bears mentioning that each of these indices is also derived from multivariate or univariate EOFs. The MEI is the time series of a multivariate EOF, based on the six main observed variables over the tropical Pacific (sea-level pressure, zonal and meridional surface winds, sea surface temperature, surface air temperature; total cloudiness fraction of the sky). A primary spatial feature captured by this index is enhanced SST along the equatorial Pacific, extending up along the west coast of

North America. The PDO is the leading principal component of North Pacific monthly sea surface temperature anomalies; the spatial pattern of the PDO entails higher SST along the coastal Northeast Pacific, with a corresponding lower SST in the deep basin. The NPGO is the second principal component of NE Pacific sea surface height anomalies, and represents a simultaneous (positively correlated) variation of the subtropical gyre (which includes the California Current system) and the subpolar gyre (which includes the Alaska Current/Alaskan Stream) of the NE Pacific.

Any number of variables could be chosen for such a multivariate analysis. Here, we wish to include the primary drivers of physical variability in the region, and the dominant response to those drivers, using only two-dimensional fields. For this purpose we include: sea surface height (SSH), temperature (SST) and salinity (SSS); mixed layer depth (SBLD); the four components of surface heat flux: latent (LATEN), sensible (SENSI), net shortwave (SW) and net longwave (LW); eastward and northward surface wind stress (USTRESS, VSTRESS); eastward and northward velocity at 40 m depth (U, V). The 40 m sampling of velocity is chosen to be deep enough to consist primarily of quasi-geostrophic flows, rather than surface wind drift; it also corresponds to numerous measurements of velocity in the GOA (Stabeno et al., this issue-a). These analysis variables are summarized in Table 1.

In many applications of univariate EOF analysis, two closely-related space and time series can indicate a propagating signal. Our particular EOF decomposition is of the form

$$Vpert(l,x,t) = X1(l,x)T1(t) + X2(l,x)T2(t) + \ldots\ldots$$

In the standard univariate case, EOF analysis can, in principle, identify a propagating wave via "fixed" spatial and temporal patterns, according to algebraic equivalence such as:

$$sin(kx\text{-}wt) = sin(kx)cos(wt) - cos(kx)sin(wt)$$

In the multivariate case with L variables, the x can be thought of as replaced by a vector x_l. This can reveal multivariate processes which are offset in space, time, or both space and time (as in the case of propagating waves).

2.3 Comparison with climate indices

For most of our comparisons between 35-year (1970-2005) EOF time series and corresponding climate time series, we calculate 12-month running means from the raw monthly values. After checking for normality, we calculate Pearson's r to test for a linear relationship between the series. Based on observed autocorrelations in the series we assume 30 degrees of freedom - that is, we assume each year is a nearly independent sample, with some allowance for autocorrelation among years. With this assumption, the 10, 5, 1, and 0.1 percent significance levels for a two-tailed t-test of r being significantly different from zero (our null hypothesis) are $|r| > 0.30$, 0.35, 0.41 and 0.45, respectively (for example, we can be 90% confident we are not obtaining a value of 0.30 for r purely by chance).

3. Results

We begin by considering the full domain of the Gulf of Alaska, and look for dominant variables and patterns in each mode. In this analysis, reference to a "strong" signal for a particular variable indicates that it has substantial magnitude relative to the standard deviation of that variable. A "weak" signal for a particular variable and location hence indicates that very little of the total variance in the original time series was explained by that mode. Our convention will be to describe the perturbation associated with the positive phase of that mode (that is, during positive values of the time series *T*). Since we are looking for coupling across variables, we limit our focus to those multivariate modes which explain more collective variance than is explained by any single variable. Since we have 12 variables total, this means we should consider only those modes which explain at least 8.5% of the total variance in our *LN* normalized time series. For the full domain, eastern GOA, and western GOA analyses, we describe only the first two modes; all others explained less than 10% of the total variance.

3.1. Annual mean spatial patterns

We begin with a summary of the climatological spatial patterns (long-term means) for each of the quantities being analyzed (Figs. 2,3). Sea surface height (SSH, 2a) is higher along the coast, in concert with the Alaskan Current/Alaskan Stream system, which intensifies in the western GOA. Sea surface temperature (SST, 2b) indicates a tongue of warm water advected from the south, with appreciable signal present all the way around the perimeter of the GOA to 160W. Sea surface salinity (SSS, 2c) reflects the input of freshwater all along the GOA coastline, with strongest input near the outflow of the Copper River. Mixed layer depth (SBLD, 2d) is deepest in the mid-shelf region of the western GOA, both east and west of Kodiak Island. It is shallowest at the northern head of the GOA, beyond the shelf break (note this is not the center of the subarctic gyre, which in fact lies to the south of the analysis domain). Latent heat loss (LATEN, 2e) is greatest offshore of the shelf break, and a slight latent heat gain is indicated for very nearshore regions. Both sensible (SENSI) and longwave (LW) heat flux losses are greatest along the shelf and near the northern head of the GOA (2f, 2g). Shortwave heat gain (SW, 2h) is greatest in the western GOA, to the southwest of Kodiak Island, and smallest offshore of the shelf break at 143W. Wind stress (USTRESS, VSTRESS, 3b) is strongest in the eastern GOA along the shelf, and weakest in the western GOA southwest of Kodiak Island. The mean currents at 40m (U, V, 3a) indicate the Alaska Current – Alaskan Stream (AS) system, with strongest flow along the shelf break in the western GOA. A deflection away from the shelf in the northeast GOA near Yakutat AK corresponds a favored site for shelf break eddy formation (Ladd et al. 2005, 2007). The ACC is present although not highly resolved in this 10 km model, and as observed in data is weak relative to the AS (Stabeno et al this volume).

3.2. Individual variable EOFs

As a preliminary to the full multivariate analysis (and as a self-consistency check on those results) we consider the first mode of variability when EOFs are calculated separately for each of the component variables of $Vpert$ (Figs. 4-6) The leading modes for SSH (4a), SBLD (4d), LATEN (4e), and LW (4g) bear a resemblance to the mean patterns for those variables, while the leading modes for SST (4b), SSS (4c), SENSI (4f) and SW (4h) are markedly different. The first modes for SST and SENSI exhibit little spatial variance; SSS has its highest amplitude in shallow enclosed regions (where ice is also sometimes formed), and SW has greatest amplitude just southeast of Kodiak Island. The first mode of U, V (6a) is greatest in the northeastern GOA. The first mode of wind stress (6b) has greatest amplitude in the western GOA. Essentially all of these univariate modes are uniform in sign, that is, all locations rise or fall together (but with varying amplitude). Modes for SST, LATEN, SENSI, LW, SW, and wind stress all explain in excess of 50% of the variance for each of those variables, while the modes for U, V explain the least (8%).

The time amplitudes of these modes are plotted together with our selected climate indices in Figs. 5-6. In general there is highest correlation with the PDO, followed by the MEI. The NPGO is only modestly correlated with any of the univariate modes ($r = -0.25$ for SST, $p>0.1$) (5b). The strongest correlations are found between SST vs. PDO (0.78, $p<.01$) (5b) and east-west wind vs. PDO (0.71, $p<.01$) (6d). Note the zero values in the perturbation time series for SW prior to 1983 (5h); this reflects the lack of data to assimilate (and hence use of climatology) for SW in the CORE reanalysis during those years. A summary of the variance explained by univariate modes, along with the r-values for each of the climate indices, is presented in Table 2.

3.3. Multivariate EOFs

We now consider the full multivariate analysis using all of the variables in Table 1 together. When the entire GOA is considered, the first two multivariate modes for *Vpert* explain 16 and 12 percent of the total variance, respectively. The higher modes explain less than 8 percent of the total variance each, and are not considered further here.

The first multivariate mode (Figs. 7-8) entails higher SSH near the coast (7a), higher SST everywhere (7b), lower SSS on the shelf (7c), deeper mixed layer SBLD in the eastern gulf and shallower SBLD in the western gulf (7d), decreased latent heat loss LATEN in the western gulf (7e) (that is, a positive perturbation on the latent heat term, which we defined as negative for heat flux out of the ocean), slightly decreased sensible heat loss SENSI (7f), decreased net longwave heat loss LW (7g), and increased northwestward wind stress, especially in the western GOA

(8b). Shortwave heat input SW (7h) and ocean velocities at 40m depth (8a) are relatively unchanged in this mode.

The second multivariate mode (Figs. 9-10) entails higher SSH beyond the shelf break (9a), enhanced SST throughout the GOA (9b), lower SSS on the shelf (9c), deeper SBLD in the eastern GOA (9d), enhanced latent heat loss in the basin (9e), enhanced sensible heat loss everywhere (9f), and enhanced shortwave heat input (9h). Neither longwave heat flux (9g) nor winds (10b) nor ocean velocities at 40m (10a) exhibit any significant signals in this mode.

The 12-month low-passed time amplitudes of modes 1 and 2 (Figs. 8c and 10c, respectively) both exhibit a significant correlation with the PDO ($r = 0.70$ and 0.70, respectively, $p<.01$) and the MEI ($r = 0.48$ and 0.53, respectively, $p<.01$), but no significant correlation with the NPGO ($r = .07$ and -.17, respectively). Weaker correlations (but a similar pattern for PDO vs. MEI vs. NPGO) are found when the 12-month filter is not applied (not shown). The two modes are distinguished by their phasing with respect to those climate indices. Coherence analysis demonstrates that the two series are most consistently coherent at super-annual frequencies, with a gradually increasing phase shift (mode 1 leads mode 2) from lower to higher frequency (Fig. 11a). This suggests a lagged correlation. Mode 1 is broadly coherent with the PDO at low frequencies, with zero phase lag (Fig. 11b); mode 2 is likewise broadly coherent with the PDO, but with an increasingly negative phase shift (PDO leads mode 2) at higher frequencies (Fig. 11c).

A simple lagged correlation analysis indicates that the time series for mode 2 is indeed significantly correlated with the time series for mode 1, when a time lag of 2-5 months is applied (r>.3, which has p<.01 if at least 100 degrees of freedom are assumed for these unfiltered monthly time series and p<.1 if we use only 30 degrees of freedom as in the yearly comparisons) (Fig. 12). Note how the two time series are completely uncorrelated at zero lag, as a consequence of EOF orthonormality.

Further inspection of these time series reveals that most of the variability in mode 1 is explained in the winter rather than the summer (Fig. 13). For mode 1, variance explained is 3x higher in the winter than the summer. For mode 2, variance explained is slightly higher in spring-summer-fall than in the winter. Together with the observed time lag between modes 1 and 2, this suggests that the combination of the modes primarily represents a sequence of events which begin in the winter and continue through the spring – for example, a warmer, wetter, windier winter, with enhanced coastal SSH, followed by a warm spring with stronger shelf-break eddies.

3.4. Multivariate EOFS on subdomains of the GOA

When multivariate EOF analysis is performed on the eastern and western GOA separately, the patterns which emerge are similar to those produced by the full GOA analysis. The mode 2 pattern for the eastern GOA is in fact very much like the mode 1 pattern for the full GOA (Figs. 14-15), as is the mode 1 pattern for the western GOA (Figs. 16-17). Similar to the findings for the full GOA (Fig. 12), we find mode 1 lags mode 2 by 2-5 months in the eastern GOA, and mode 2 lags mode 1 by 2-5 months in the western GOA (not shown). Certain aspects of the time-leading spatial pattern are enhanced in each case. In the eastern GOA, the elevated coastal SSH

(14a) and deeper SBLD (14d) have strong signals and show a similar spatial pattern to each other, in association with broadly enhanced SST (14b) and northwestward winds (15b). The eastern GOA mode 2 time series exhibits a correlation of 0.76, 0.54 and 0.04 with the PDO, MEI and NPGO, respectively (15c). Similarly, the western GOA mode 1 pattern strongly mimics the full GOA mode 1 pattern, in particular with shallower SBLD in the eastern half and deeper SBLD in the west (16d). In this case the time series exhibits a correlation of 0.66, 0.47 and 0.02 with the PDO, MEI and NPGO, respectively (17c). A summary of the variance explained by multivariate modes, along with the r-values for each of the climate indices, is presented in Table 3.

3.5 Formation and spinoff of shelf-break eddies

A full interpretation of the multivariate results assumes that the model properly forms and evolves shelf-break eddies. Here we compare model features with altimeter data as a check on performance. Both model and data exhibit approximately the same number of 200-km eddy features during the eddy-rich period of April 15 1998 (Fig. 18 a,b), but the model produces these in slightly different locations and at smaller amplitude than the data. A comparison of EKE time series (Fig. 18c) demonstrates a strong correspondence during the major El Nino event of 1997-1998, as well as the weaker events of 94-95 and 02-03, with moderate correlation (similar pattern but smaller amplitude) between those periods (r ~ 0.6 for the total series). In conjunction with the model-data comparisons of Danielson et al. (2012) and Hermann et al. (2013, 2015), these results serve to demonstrate how the model, driven by observed (reanalyzed) CORE atmospheric fields, captures much of the interannual variation of both mean currents and eddy statistics (e.g. the size and number of shelf-break eddies formed in a given year). The failure of the model to replicate the finer-scale details of the eddies derives from the chaotic nature of eddy dynamics, and the lack of any mesoscale oceanic data assimilation in this particular simulation.

Our primary multivariate modes, lagged by 2-5 months as shown in Fig. 12, appear to contain this eddy formation/detachment dynamic. The EOF spatial patterns for SSH in both eastern and western regions entail higher SSH onshore under the time-leading mode (specifically, mode 2 for the eastern GOA [12d] and mode 1 for the western GOA [12f]), and higher SSH beyond the shelf break under the time-following mode (mode 1 for the eastern GOA [12e] and mode 2 for the western GOA [12g]). The time-following modes (12e,g) include mesoscale patterns suggestive of the shelf-break eddies and their typical formation regions (Ladd et al. 2007).

4. Discussion

4.1 What do these modes suggest?

Clearly there is strong association with the PDO/MEI in these leading modes of variability of our model output. Together these modes suggest the following wintertime events during periods of positive PDO/MEI: 1) anomalously warm, wet and windy conditions, with elevated coastal SSH, followed 2-5 months later by 2) reduced cloud cover, with emerging shelf-break eddies. Similar modes are found when the EOF calculation is performed separately on the eastern and western GOA. In general, modal amplitudes appear stronger in the western GOA. Both of the modes include deeper MLD and reduced SSS during their positive phase; these particular signals are strongest in the eastern GOA.

These model-based analyses are broadly consistent with the conclusions of Janout et al (2010, 2013), which underscored the importance of wintertime cooling to subsequent temperatures in the GOA. Based on these general features we propose the following chain of events during positive PDO/ENSO events:

Mode 1: Enhanced northwestward winds increase the wind speed in the east but depress total wind speed in the west, where the mean winds are southeastward. This leads to greater SSH along the coast, and alternately deeper/shallower mixed layer in the eastern/western GOA. Atmospheric conditions broadly raise the SST. The increased winds do not substantially alter the currents at 40m depth; possibly this is due to the spatial pattern of the perturbation, as it has smallest amplitude along the coast of the eastern GOA and hence reduced ability to generate Coastal Trapped Waves there. Reduced net longwave heat loss in the west, along with the reduced latent heat loss, may be a function of the wetter conditions there during MEI/PDO events (as increased atmospheric moisture results in more longwave irradiance to the ocean surface).

Mode 2 (following 2-5 months after mode 1): Winds drop back to their average levels. Enhanced shortwave irradiance (reduced cloud cover) heats the ocean surface to such a degree that sensible heat loss is increased. The sunnier (and presumably dryer) conditions also lead to enhanced latent heat loss. The enhanced coastal SSH during Mode 1 spins off as large shelf-break eddies, particularly in the eastern GOA; this is consistent with the conclusions of Combes et al. (2009) and Hermann et al. (2009). In addition, while not resolved by this model, Ladd and Cheng (this issue) noted a correlation between ENSO and gap wind frequency in the eastern GOA. Since gap winds events can result in eddies, that may be an additional mechanism by which ENSO is connected with eddy formation.

Given the strong correlations observed with the PDO/MEI, we have not identified truly independent dynamics local to the GOA in these first two modes. The GOA is a small portion of the North Pacific and hence unlikely to feed back significantly on the atmosphere at these scales; it is more "driven" than "driver" in this sense. It remains possible that locally-governed modes of variability are lurking in some of the higher modes from our analysis, but they apparently explain little of the total variance for our chosen variables. We must emphasize that: 1) these results are dependent on the spatial scales of the analysis (which exclude regional scale processes such as gap winds); and 2) by construction, EOF analysis will typically render large scale patterns, as they tend to explain more of the total variance over any broad spatial domain than will small, regionally focused patterns.

Although the present analysis only goes through 2005, the strong correlation of the modes with the PDO/MEI suggests multivariate behavior in the 2011 and 2013 field years of the GOAIERP program. During 2011-2013, the PDO was in a largely negative phase (http://jisao.washington.edu/pdo/), while the MEI was negative during 2011, and fluctuated between positive and negative values during 2013 (http://www.esrl.noaa.gov/psd/enso/mei/). According to our analysis, this suggests the co-occurrence of a drier than normal winter with reduced northwestward wind stress, cooler than normal SST, and lower than normal coastal SSH during 2011, with more average conditions during 2013.

4.2 Variance explained by univariate vs. multivariate modes

The univariate EOF modes each explain more of the total variance in that variable (typically > 50% for the first mode), than any of the multivariate modes can explain for the collected variables (16% for the first mode). This is a fully expected result – for one thing, not all of the variables will necessarily be covariant in time with the others in a multivariate analysis. In the extreme case, consider 12 different variables on the same spatial grid, each fully captured by a single mode in univariate EOF analysis. If the time amplitudes of these single modes were all mutually orthogonal, a multivariate EOF analysis would not be able to link them together. Indeed, in the multivariate analysis they might appear as a collection of 12 different modes, each explaining only ~8.5% of the total variance, but each explaining 100% of the variance of a single variable.

4.3 Relationship to the NPGO

With one exception (first multivariate mode for the eastern GOA) we found no strong correlation between the NPGO and any of our model-derived modes, either univariate or multivariate, at either monthly or yearly timescales. A weak correlation (r=0.27) does exist between the first univariate mode for northward wind stress and the NPGO (Fig. 4), but the equivalent correlation for all other variables was even lower. To some degree this may reflect slower dynamics at work in the NPGO relative to MEI and PDO, as it is based on SSH and may be influenced by processes with appreciable time lag such as westward-propagating Rossby waves originating at the eastern boundary. Indeed, it is readily apparent from the figures that the NPGO has a redder spectrum (predominance of lower frequencies) relative the MEI, PDO, or the modal time series themselves. Further, the spatial map of the NPGO itself (DiLorezo et al., 2008) projects less strongly onto the coastal GOA than it does onto other regions of the Northeast Pacific. Capotondi et al. (2009) have noted a much stronger correlation of the NPGO with subsurface features such as pycnocline depth to the southeast of our domain, however.

4.4 Other possible climate indices

For comparison with climate indices, we included only the PDO, MEI and NPGO. There are of course many other standard climate indices we could explore. In particular the strength and location of the Aleutian Low has been noted as a major determinant of GOA conditions. Typically, positive ENSO and PDO events are associated with an intensification of the Aleutian Low (Weingartner, 2007). A visual inspection of the North Pacific index of Trenberth and Hurrell (1994) (https://climatedataguide.ucar.edu/climate-data/north-pacific-np-index-trenberth-and-hurrell-monthly-and-winter) suggests a weaker correlation with our modal time series than either the PDO or MEI; however, further inspection of such additional climate time series may reveal other informative correlations with aggregate GOA behavior.

4.5 Connection to subsurface velocity

The weak loading of either 40 m velocity component on any of the multivariate modes was surprising; we might have expected a stronger covariance to emerge, given the strong loading of wind stress. A stronger covariance would doubtless emerge if we were to use velocities at the surface, rather than at depth. It is also possible that a lagged multivariate covariance exists between 40 m velocity and the other variables. The first univariate mode for velocity clearly reflects changes in the strength of the Aleutian Stream (see Fig. 3), even though it accounts for only ~8% of the total variance over the total domain, and the east-west velocity is significantly correlated with the PDO ($r=-0.32$, $p<0.10$). The Alaskan Stream is sometimes described as having relatively low variability; because it is a western boundary current along much of its path, and because it is offshore, it does not respond as quickly to local winds as does the ACC (which is both weaker in nature and only marginally resolved in our 10 km model, hence contributing less than the Alaskan Stream to the total variance). While it exhibits no strong pattern of flow at 40m, the SSH anomaly of multivariate mode 1 does suggest enhanced overall circulation around the subarctic gyre, as it strengthens the mean condition of higher SSH along the coast relative to the basin (Fig. 2). This signal may well be related to changes in wind stress curl, and merits further analysis.

4.6 Limitations and possible improvements

The analysis technique used here is of course only one among many possible. A different choice of variables and spatial domain (e.g. one focused exclusively on the continental shelf) would emphasize different features of the regional dynamics, and a finer-resolution model would better resolve the ACC, which is only marginally captured here. The CORE winds used do not include fine-scale orographic effects such as gap winds (Ladd et al. this issue) or other coastal atmospheric phenomena (Stabeno et al., 2004; Winstead et al. 2006), but previous sensitivity studies have suggested these are not essential to capture the ACC in the northern GOA (Dobbins et al. 2009).

The use of an ocean model driven by an atmospheric reanalysis may tend to overemphasize certain heat fluxes, as the imposed atmosphere cannot come into local balance with the evolving regional ocean dynamics – that is, while the true atmosphere felt and responded to the evolution of the true ocean, our imposed atmospheric forcing never feels and responds to the (possibly different) evolution of our modeled ocean. In our case, this lack of two-way feedback may tend to overemphasize the flux of sensible heat from the ocean to the atmosphere during some periods. Note, however, that the CORE reanalysis used to drive our regional model includes all the true feedbacks between the (coarsely-resolved) global ocean and the atmosphere, as it is derived from true oceanic and atmospheric data. Hence, provided that our regional model reproduces the observed coarse-scale SST and currents, the only feedbacks we are truly missing here are those between the fine-scale oceanic features resolved by the model and the overlying (and here coarsely resolved) atmosphere. These are of much smaller consequence than the large-scale feedbacks, especially during periods of strong winds, since there is very little time for interaction between a swiftly advecting air mass and any small patch of the ocean.

Possibly the most significant element missing from our analysis thus far is the interannual variation of runoff forcing to the coastal GOA; while changes in precipitation are included in the CORE forcing, the coastal runoff applied to the NEP-5 simulation was climatological. The MEI and coastal runoff anomalies are in fact correlated during some (but not all) periods: i.e. more/less runoff in El Nino/La Nina years. A fine-scale (3 km) resolution biophysical model of the coastal GOA developed under the GOAIERP program includes these variations, and multivariate analysis of that output will be reported separately. The lack of spatial detail in our runoff forcing is also problematic, and underestimates the impact of runoff in areas such as Prince William Sound. Anticipated fine-scale biophysical simulations will include more finely resolved products (e.g. Hill et al. 2015).

5. Summary and conclusions

A multivariate EOF analysis of output from a physical model of the Gulf of Alaska reveals two modes, both substantially correlated with PDO/MEI indices, which together account for ~30% of the total variance of the perturbation time series. As expected, the leading modes here do not in general explain as much variance as a corresponding univariate EOF analysis; however, unlike simple univariate analysis they serve as a summary of covariant spatial behavior in the GOA, and suggest a sequence of events correlated across different sets of variables. In particular, these two modes suggest the following events during periods of positive PDO/MEI: 1) anomalously warm, wet and windy conditions during winter, with elevated coastal SSH, followed 2-5 months later by 2) reduced cloud cover, with emerging shelf-break eddies. Similar modes are found when the EOF calculation is performed separately on the eastern and western GOA. In general, modal amplitudes appear stronger in the western GOA. Ultimately this type of analysis aids the interpretation of biological variability of the GOA, as the ecosystem experiences these coupled physical phenomena.

Acknowledgements

This research is contribution No. 4284 from NOAA/Pacific Marine Environmental Laboratory, and contribution Eco-FOCI-0839 to NOAA's Ecosystems Fisheries Oceanography Coordinated Investigations. This publication is partially funded by the Joint Institute for the Study of the Atmosphere and Ocean (JISAO) under NOAA cooperative agreement NA10OAR4320148, Contribution No. 2533. The research was generously supported by the North Pacific Research Board (NPRB) sponsored Gulf of Alaska Integrated Ecosystem Research Program and NOAA's North Pacific Climate Regimes and Ecosystem Productivity programs. This is Gulf of Alaska

Project publication number XX, supported by the North Pacific Research Board through Project XX.

Table 1. Variables used in the statistical analysis.

Category	Variable name	Description	Units
Ocean Scalars			
	SSH	sea surface height	m
	SST	Sea surface temperature	^{o}C
	SSS	Sea surface salinity	psu
	SBLD	Mixed layer depth	m
Heat Flux			
	LATEN	Latent heat flux	W m^{-2}
	SENSI	Sensible heat flux	W m^{-2}
	LW	Net longwave heat flux	W m^{-2}
	SW	Shortwave heat flux	W m^{-2}
Wind Stress			
	USTRESS	Eastward wind stress	N m^{-2}
	VSTRESS	Northward wind stress	N m^{-2}
Ocean Velocity			
	U	Eastward 40 m velocity	m s^{-1}
	V	Northward 40 m velocity	m s^{-1}

Table 2. Statistics of the first univariate mode for each of the variables in Table 1. Percent variance explained by the first univariate mode, and the r-value for correlation of the corresponding time series with climate indices.

		r value		
Variable	Percent variance explained	MEI	PDO	NPGO
SSH	39.5	+0.27	+0.44	-0.04
SST	66.8	+0.61	+0.78	-0.25
SSS	44.9	+0.46	+0.66	+0.04
SBLD	32.3	+0.24	+0.35	+0.08
LATEN	63.3	+0.19	+0.20	-0.06
SENSI	65.1	+0.43	+0.55	-0.18
LW	70.3	+0.35	+0.53	+0.13
SW	55.5	+0.21	+0.27	-0.19
U	8.7*	-0.22	-0.32	+0.28
V		+0.18	-0.03	-0.12
USTRESS	74.4*	+0.46	+0.71	-0.09
VSTRESS		+0.32	+0.34	+0.27

* average percent explained for u- and v-components

Table 3. Statistics of the first two multivariate modes for the full GOA, the eastern GOA, and the western GOA. Percent variance explained by the mode, and the r-value for correlation of the corresponding time series with climate indices

		r-value		
Region and Mode	Percent variance explained	MEI	PDO	NPGO
Full GOA 1	16.7	+0.48	+0.70	+0.07
Full GOA 2	12.4	+0.53	+0.70	-0.17
East GOA 1	14.7	+0.37	+0.39	-0.41
East GOA 2	13.9	+0.54	+0.76	+0.04
West GOA 1	20.1	+0.47	+0.66	+0.02
West GOA 2	13.4	+0.47	+0.65	-0.13

References

Bretherton, C.S., Smith, C., Wallace, J.M., 1992. An intercomparison of methods for finding coupled patterns in climate data. J. Clim. 5, 541-560.

Budgell, W.P., 2005. Numerical simulation of ice-ocean variability in the Barents Sea region: Towards dynamical downscaling, Ocean Dynamics, 55: 370-387

Capotondi, A., Combes, V., Alexander, M. A., Di Lorenzo, E., Miller, A.J., 2009. Low-frequency variability in the Gulf of Alaska from coarse and eddy-permitting ocean models. Journal of Geophysical Research-Oceans, 114, doi:10.1029/2008jc004983.

Combes, V., Di Lorenzo, E., Curchitser, E., 2009. Interannual and Decadal Variations in Cross-Shelf Transport in the Gulf of Alaska. Journal of Physical Oceanography, 39(4) 1050-1059, doi:10.1175/2008jpo4014.1.

Curchitser, E.N., Hedstrom, K., Danielson, S. and Weingartner, T.J., 2010. Modeling of circulation in the North Aleutian Basin, OCS Study BOEMRE 2010-028, Bureau of Ocean Management., U.S. Department of the Interior, Washington, D. C. [Available at http://alaska.boemre.gov/reports/2010rpts/2010_028.pdf.]

Dai, A., Qian, T., Trenberth, K. E., Milliman, J. D, 2009. Changes in continental freshwater discharge from 1948-2004. J. Climate 22, 2773-2791.

Danielson, S., Curchitser, E., Hedstrom, K., Weingartner, T., Stabeno, P., 2011. On ocean and sea ice modes of variability in the Bering Sea. J. Geophys. Res., 116, C12034, doi:10.1029/2011JC007389.

Di Lorenzo, E., J. Fiechter, N. Schneider, A. Bracco, A. J. Miller, P. J. S. Franks, S. J. Bograd, A. M. Moore, A. C. Thomas, W. Crawford, A. Pena and A. J. Hermann, 2009: Nutrient and salinity decadal variations in the central and eastern North Pacific. Geophysical Research Letters, 36, doi:10.1029/2009gl038261.

Di Lorenzo, E., N. Schneider, K. M. Cobb, P. J. S. Franks, K. Chhak, A. J. Miller, J. C. McWilliams, S. J. Bograd, H. Arango, E. Curchitser, T. M. Powell and P. Riviere, 2008: North Pacific Gyre Oscillation links ocean climate and ecosystem change. Geophysical Research Letters, 35(8), doi:10.1029/2007gl032838.

Haidvogel, D.B., Arango, H., Budgell, W.P., Cornuelle, B.D., Curchitser, E., Di Lorenzo, E., Fennel, K., Geyer, W.R., Hermann, A.J., Lanerolle, L., Levin, J., McWilliams, J. C., Miller, A. J., Moore, A.M., Powell, T.M., Shchepetkin, A.F., Sherwood, C.R., Signell, R.P., Warner, J.C., Wilkin, J., 2008. Regional Ocean Forecasting in Terrain-following Coordinates: Model Formulation and Skill Assessment. J. Comput. Phys. 227, 3595-3624.

Hermann, A. J., E. N. Curchitser, D. B. Haidvogel and E. L. Dobbins, 2009. A comparison of remote versus local influence of El Nino on the coastal circulation of the Northeast Pacific. Deep Sea Research II, doi:10.1016/j.dsr2.2009.02.005.

Hermann, A. J., Gibson, G.A., Bond, N.A., Curchitser, E.N., Hedstrom, K., Cheng, W., Wang, M., Stabeno, P.J., Eisner, L., Cieciel, K.D., 2013. A multivariate analysis of observed and modeled biophysical variability on the Bering Sea shelf: multidecadal hindcasts (1970-2009) and forecasts (2010-2040). Deep Sea Research II, 94:121-139, doi:10.1016/j.dsr2.2013.04.007

Hermann, A. J., G. A. Gibson, N. A. Bond, E. N. Curchitser, K. Hedstrom, W. Cheng, M. Wang, E. D. Cokelet, P. J. Stabeno and K. Aydin, 2015. Projected future biophysical states of the Bering Sea. Deep-Sea Research II. http://dx.doi.org/10.1016/j.dsr2.2015.11.001

Hill, D. F., N. Bruhis, S. E. Calos, A. Arendt, and J. Beamer, 2015. Spatial and temporal variability of freshwater discharge into the Gulf of Alaska, J. Geophys. Res. Oceans, 120, 634–646, doi:10.1002/2014JC010395.

Janout, M.A., Weingartner, T.J., Royer, T. C., Danielson, S. L., 2010. On the nature of winter cooling and the recent temperature shift on the northern Gulf of Alaska shelf, JGR Oceans, 2009JC005774R, DOI: 10.1029/2009JC005774

Janout, M. A., Weingartner, T. J., Stabeno, P. J., 2013. Air-sea and oceanic heat flux contributions to the heat budget of the northern Gulf of Alaska shelf, Journal of Geophysical Research-Oceans. doi:10.1002/jgrc.20095

Ladd, C., 2007. Interannual variability of the Gulf of Alaska eddy field. *Geophys. Res. Lett.*, *34*(11), L11605, doi: 10.1029/2007GL029478

Ladd, C., Kachel, N.B., Mordy, C.W., Stabeno, P.J., 2005. Observations from a Yakutat eddy in the northern Gulf of Alaska. Journal of Geophysical Research—Oceans 110 (C3), C03003.

Ladd, C., Mordy, C.W., Kachel, N.B., Stabeno, P.J., 2007. Northern Gulf of Alaska eddies and associated anomalies. Deep-Sea Research Part I 54 (4), 487–509.

Ladd, C., Cheng, W., Salto, S., this issue. Gap Winds near Kodiak Island, Alaska and effects on regional oceanography. Deep-Sea Res. II.

Ladd, C., Cheng, W., this issue. Characteristics of "Gap Winds" from Cross Sound, Alaska and their effects on regional oceanography. Deep-Sea Res. II.

Large, W.G., McWilliams, J.C., Doney, S.C., 1994. Oceanic vertical mixing: a review and a model with a nonlocal boundary layer parameterization, Rev. Geophys. 32, 363-403.

Large, W.G., Yeager, S.G., 2008. The global climatology of an interannually varying air-sea 1009 flux data set, Clim. Dyn. 33, 341-364

Mantua, Nathan J., Steven R. Hare, Yuan Zhang, John M. Wallace, and Robert C. Francis, 1997: A Pacific Interdecadal Climate Oscillation with Impacts on Salmon Production. *Bull. Amer. Meteor. Soc.*, **78**, 1069–1079.

Melsom, A., Metzger, E.J., Hurlburt, H.E., 2003. Impact of remote oceanic forcing on Gulf of Alaska sea levels and mesoscale circulation. J. Geophys. Res. - Oceans 108, 3346. doi:10.1029/2002JC001742.

Melsom, A., Meyers, S.D., Hurlburt, H.E., Metzger, J.E., O'Brien, J.J., 1999. ENSO effects on Gulf of Alaska eddies. Earth Interactions 3, 1-30.

Murray, C.P., Morey, S.L., O'Brien, J.J., 2001. Interannual variability of upper ocean vorticity balances in the Gulf of Alaska. J. Geophys. Res. - Oceans 106, 4479-4491.

Okkonen, S.R., Jacobs, G.A., Metzger, E.J., Hurlburt, H.E., Shriver, J.F., 2001. Mesoscale variability in the boundary currents of the Alaska Gyre. Cont. Shelf Res. 21, 1219-1236.

Parada, C, Hinckley, S., Horne, J., Mazur, M., Dorn, M., Hermann, A., Curchitser, E., this issue. Modeling connectivity of walleye pollock in the Gulf of Alaska: Are there any linkages to Bering Sea and Aleutian Islands? Deep-Sea Res. II.

Shchepetkin, A.F., McWilliams, J.C., 2005. The regional oceanic modeling system (ROMS): a split-explicit, free-surface, topography-following-coordinate oceanic model, Ocean Modelling 9 (4), 347-404.

Stabeno, P.J., Bond, N.A., Hermann, A.J., Kachel, N.B., Mordy, C.W., Overland J.E., 2004. Meteorology and oceanography of the northern Gulf of Alaska. Cont. Shelf Res., 24, doi: 10.1016/j.csr.2004.02.007, 859–897.

Stabeno, P.J., Bell, S., Cheng, W., Danielson, S., Kachel, N.B., Mordy, C.W., this issue-a. Long-term observations of Alaska Coastal Current in the northern Gulf of Alaska. Deep-Sea Res. II.

Stabeno, P.J., Bond, N.A., Kachel, N.B., Ladd, C., Mordy, C., Strom, S.L., this issue-b. Southeast Alaska: Currents, mixing and chlorophyll-a. Deep-Sea Res. II.

Weingartner, T. Agents of Ecosystem Change, Climate, pp. 171 – 178 in R. Spies (ed.), Long-Term Ecological Change in the Northern Gulf of Alaska, Elsevier, Oxford, UK, 589 p., 2007.

Winstead, N. S., B. A. Colle, N. Bond, G. Young, J. Olson, K. Loescher, F. Monaldo, D. Thompson, and W. Pichel, 2006. Barrier Jets: Combining SAR Remote Sensing, Field Observations and Models to Better Understand Coastal Flows in the Gulf of Alaska, *Bull. Amer. Meteor. Soc.*, 87, 787-800.

Wolter, K., and M.S. Timlin, 1993: Monitoring ENSO in COADS with a seasonally adjusted principal component index. *Proc. of the 17th Climate Diagnostics Workshop*, Norman, OK, NOAA/NMC/CAC, NSSL, Oklahoma Clim. Survey, CIMMS and the School of Meteor., Univ. of Oklahoma, 52-57.

Wolter, K., and M. S. Timlin, 1998: Measuring the strength of ENSO events - how does 1997/98 rank? *Weather,* **53,** 315-324.

List of Figures

Figure 1. ROMS-NEP numerical model domain with bathymetry (shaded, m). Full Gulf of Alaska domain used for statistical analysis is shown by black line. The red line denotes separator (at 145W) between east and west subsections used for analysis. Blue line indicates location of hydrographic line P. Green box indicates the domain of the EKE analysis (56.5-58N, 139-136W). Figure modified from Danielson et al. (2011).

Figure 2. Annual average spatial fields from the model. a) SSH = sea surface height (m); b) SST = sea surface temperature (deg C); c) SSS = sea surface salinity (psu); d) SBLD = mixed layer depth (negative z indicates m below the sea surface); e) LATEN, f) SENSI, g) LW, h) SW = latent, sensible, net longwave and net shortwave heat flux (W m-2, positive denotes flux into the ocean);). Copper River outflow is at 60.5N, 145W.

Figure 3. Annual average spatial fields from the model. a) uv = velocity at 40m depth (shading denotes speed in m s-1); b) uvstress = surface wind stress in N m-2 (shading denotes stress vector magnitude.

Figure 4. First spatial modes from univariate EOF analyses based on perturbations from monthly climatology. Variables and units are as in Figure 2. Percent of total variance explained by the first mode for each variable is shown (pcvar).

Figure 5. Low-passed (12-month running mean) time series for each of the first mode univariate EOFs shown in Figure 4 (black lines). Also plotted are low-passed MEI (red lines), PDO (green lines) and NPGO (light blue lines) time series.

Figure 6. First spatial modes from univariate EOF analyses based on perturbations from monthly climatology: a) uv = velocity at 40m depth (shading denotes speed in m s-1); b) uvstress = surface wind stress in N m-2 (shading denotes stress vector magnitude). Low-passed (12-month running mean) time series for the first mode of: c) u and v at 40m; d) surface wind stress. For c) and d), solid line is u-component and dashed line is v-component. Also plotted are low-passed MEI (red lines), PDO (green lines) and NPGO (light blue lines) time series.

Figure 7. First mode spatial patterns from the multivariate EOF analysis of the Gulf of Alaska. Variable definitions and units are as in Figure 2. Color palettes are chosen to span +/- 0.5 of the standard deviation of the original variable.

Figure 8. First mode spatial patterns for the multivariate EOF analysis; results for a) velocity at 40m depth and b) surface wind stress. Variable units as in Figure 6. c) Low-pass filtered (12-month running mean) time amplitude of the multivariate mode (black line) as compared with the MEI (red line), PDO (green line), and NPGO (light blue line) climate indices. Color palettes are chosen to span +/- 0.5 of the standard deviation of the original variable.

Figure 9. As in Fig. 7, for the second multivariate mode from the EOF analysis of the Gulf of Alaska.

Figure 10. As in Fig. 8, for the second multivariate mode from the EOF analysis of the Gulf of Alaska.

Figure 11. Raw monthly time series with frequency spectra, coherence and phase lag for: a) full GOA mode 1 (black) vs. mode 2 (red); b) full GOA mode 1 (black) vs. PDO (red); c) full GOA mode 2 (black) vs. PDO (red). Red, green, blue lines indicate 90%, 95%, 99% confidence levels, respectively, for coherence significantly different than zero.

Figure 12. Correlation (r-value) between multivariate modes 1 and 2 as a function of time lag (months). Positive lag indicates mode 2 is lagged relative to mode 1.

Figure 13. RMS amplitude of the multivariate EOF time series for the Gulf of Alaska as a function of month. Shown are results for mode 1 (solid line), mode 2 (dashed line).

Figure 14. As in Fig. 7, for the second multivariate mode from the EOF analysis of the eastern Gulf of Alaska.

Figure 15. As in Fig. 8, for the second multivariate mode from the EOF analysis of the eastern Gulf of Alaska.

Figure 16. As in Fig. 7, for the first multivariate mode from the EOF analysis of the western Gulf of Alaska.

Figure 17. As in Fig. 8, for the first multivariate mode from the EOF analysis of the western Gulf of Alaska.

Figure 18. EKE analyses and correspondence to EOF results. a) SSH anomaly relative to long-term mean from model output on April 15, 1998. b) SSH anomaly from altimeter data on this date. Black outlines indicate the area used for EKE comparison. c) EKE time series for data (black line) vs. model (red line). Also shown are multivariate EOF modes for SSH in the eastern and western GOA. These illustrate evolution from: d) higher coastal SSH in the eastern GOA (mode 2), followed by e) offshore SSH with mesoscale pattern (mode 1); f) higher coastal SSH in the western GOA (mode 1), followed by f) offshore SSH with mesoscale pattern in the western GOA (mode 2). A lagged correlation of these phenomena is similar to that for the entire GOA, illustrated in Figure 12.

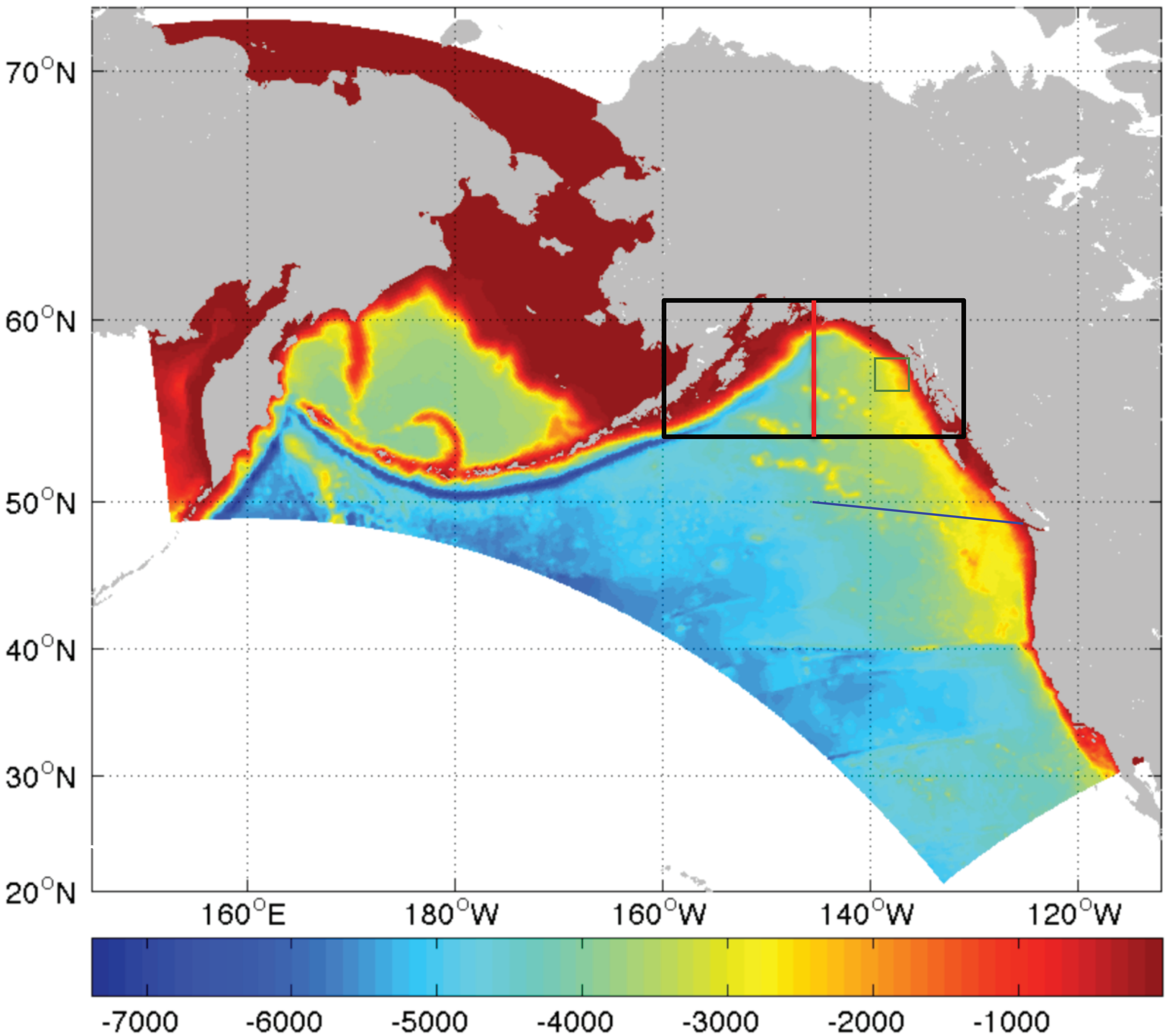

70°N
60°N
50°N
40°N
30°N
20°N
160°E
180°W
160°W
140°W
120°W
-7000
-6000
-5000
-4000
-3000
-2000
-1000

Figure 1

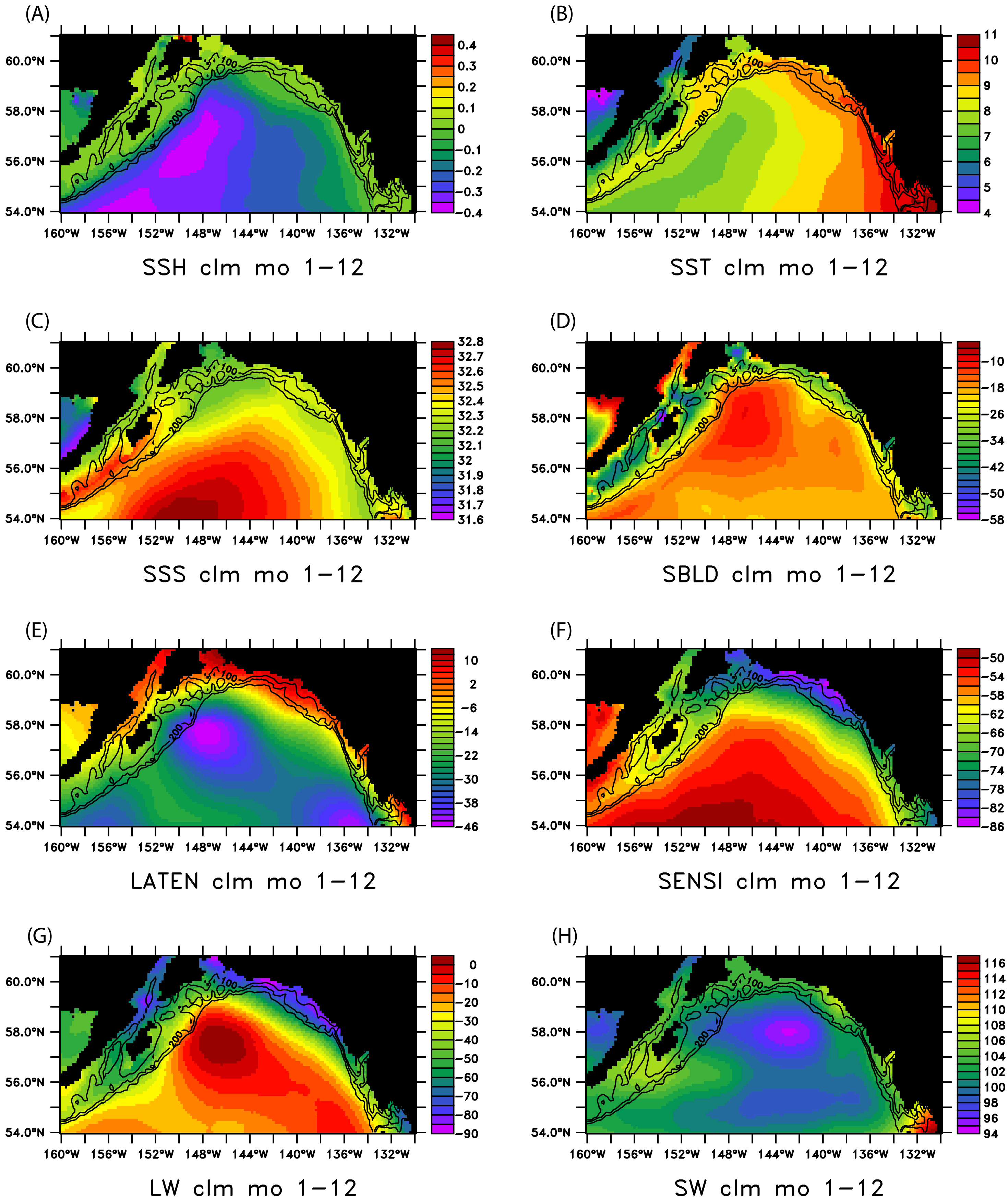

(A)
SSH clm mo 1−12
0.4
0.3
0.2
0.1
0
−0.1
−0.2
−0.3
−0.4
(B)
SST clm mo 1−12
11
10
9
8
7
6
5
4
(C)
SSS clm mo 1−12
32.8
32.7
32.6
32.5
32.4
32.3
32.2
32.1
32
31.9
31.8
31.7
31.6
(D)
SBLD clm mo 1−12
−10
−18
−26
−34
−42
−50
−58
(E)
LATEN clm mo 1−12
10
2
−6
−14
−22
−30
−38
−46
(F)
SENSI clm mo 1−12
−50
−54
−58
−62
−66
−70
−74
−78
−82
−86
(G)
LW clm mo 1−12
0
−10
−20
−30
−40
−50
−60
−70
−80
−90
(H)
SW clm mo 1−12
116
114
112
110
108
106
104
102
100
98
96
94
60.0°N
58.0°N
56.0°N
54.0°N
160°W
156°W
152°W
148°W
144°W
140°W
136°W
132°W
100
200

Figure 2

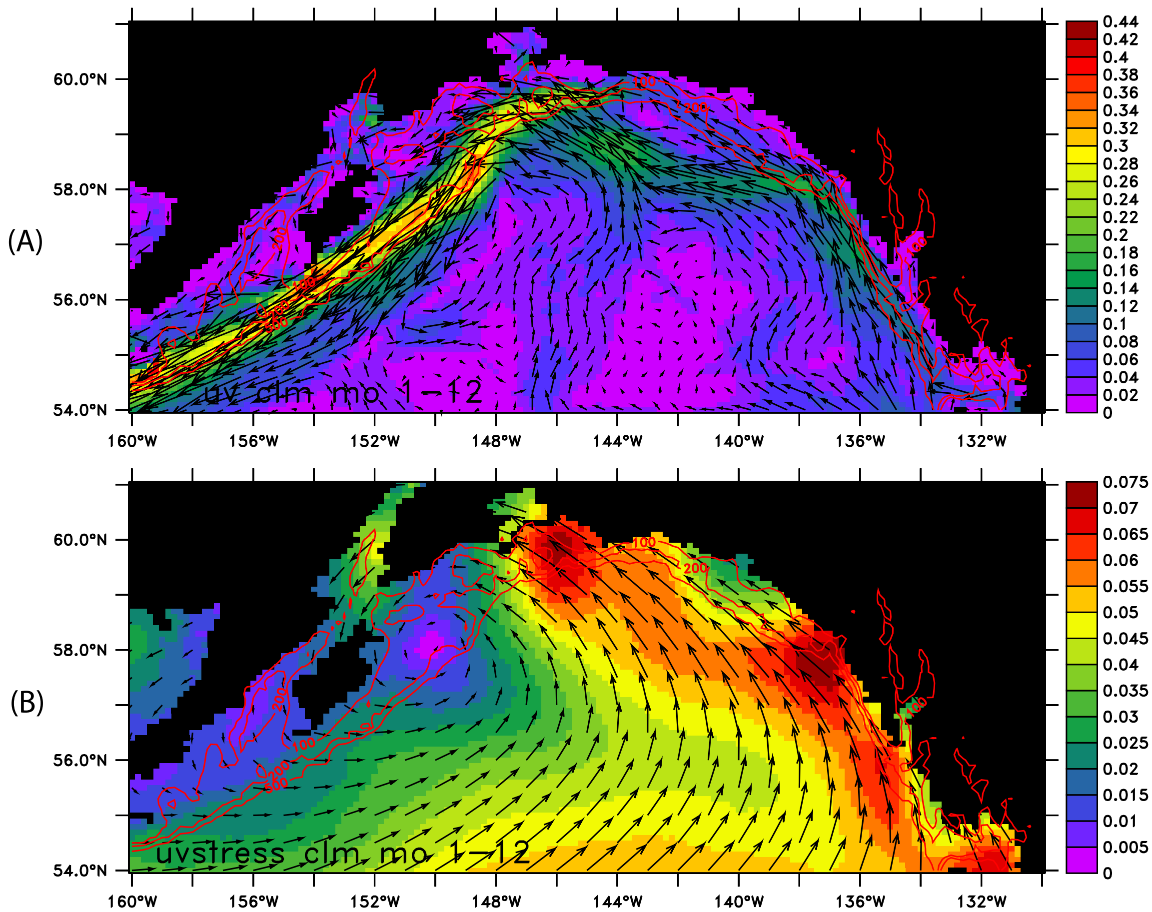
(A)
uv clm mo 1-12
(B)
uvstress clm mo 1-12
60.0°N
58.0°N
56.0°N
54.0°N
160°W
156°W
152°W
148°W
144°W
140°W
136°W
132°W

Figure 3

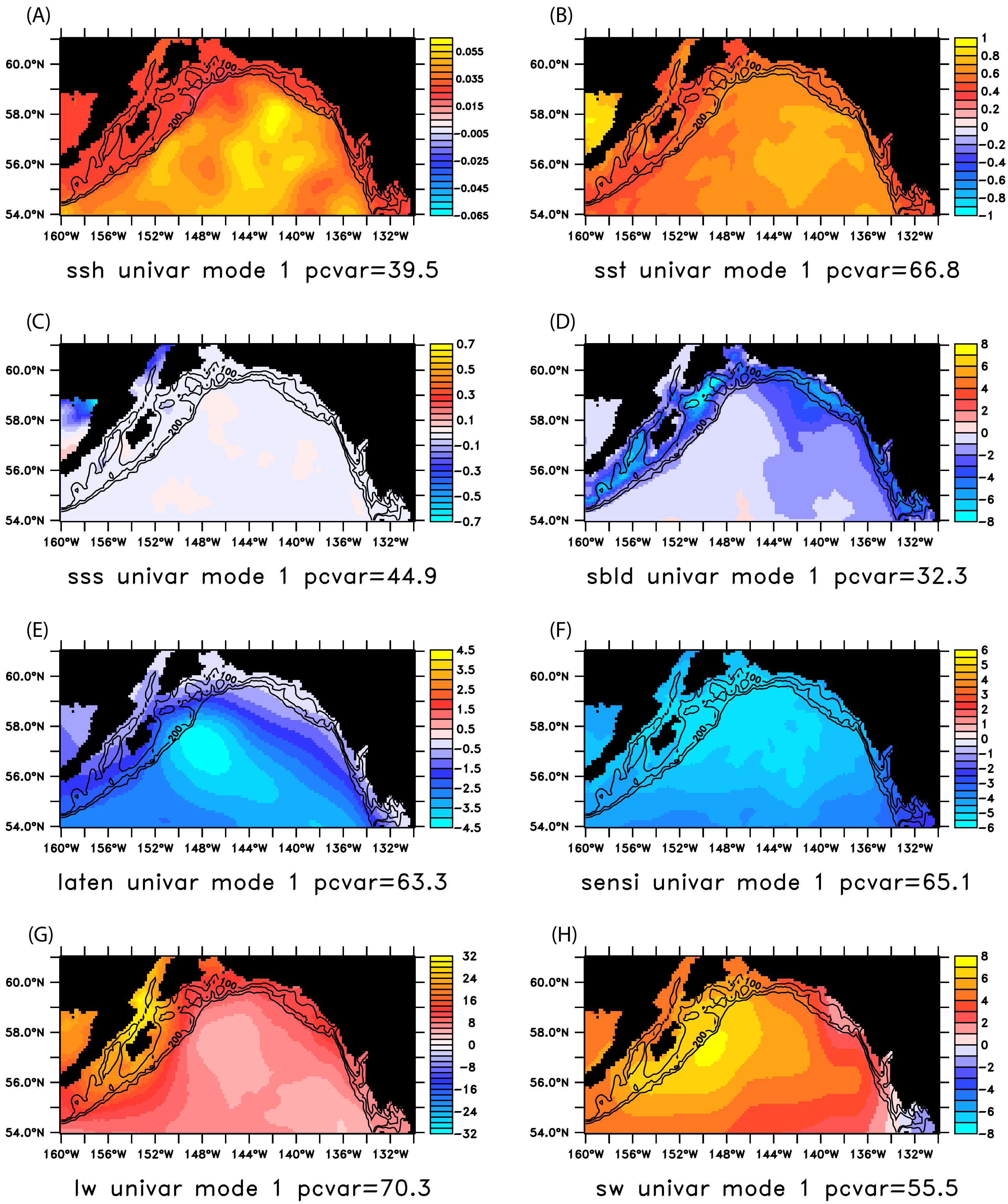
(A)
ssh univar mode 1 pcvar=39.5
(B)
sst univar mode 1 pcvar=66.8
(C)
sss univar mode 1 pcvar=44.9
(D)
sbld univar mode 1 pcvar=32.3
(E)
laten univar mode 1 pcvar=63.3
(F)
sensi univar mode 1 pcvar=65.1
(G)
lw univar mode 1 pcvar=70.3
(H)
sw univar mode 1 pcvar=55.5
60.0°N
58.0°N
56.0°N
54.0°N
160°W 156°W 152°W 148°W 144°W 140°W 136°W 132°W
100
200

Figure 4

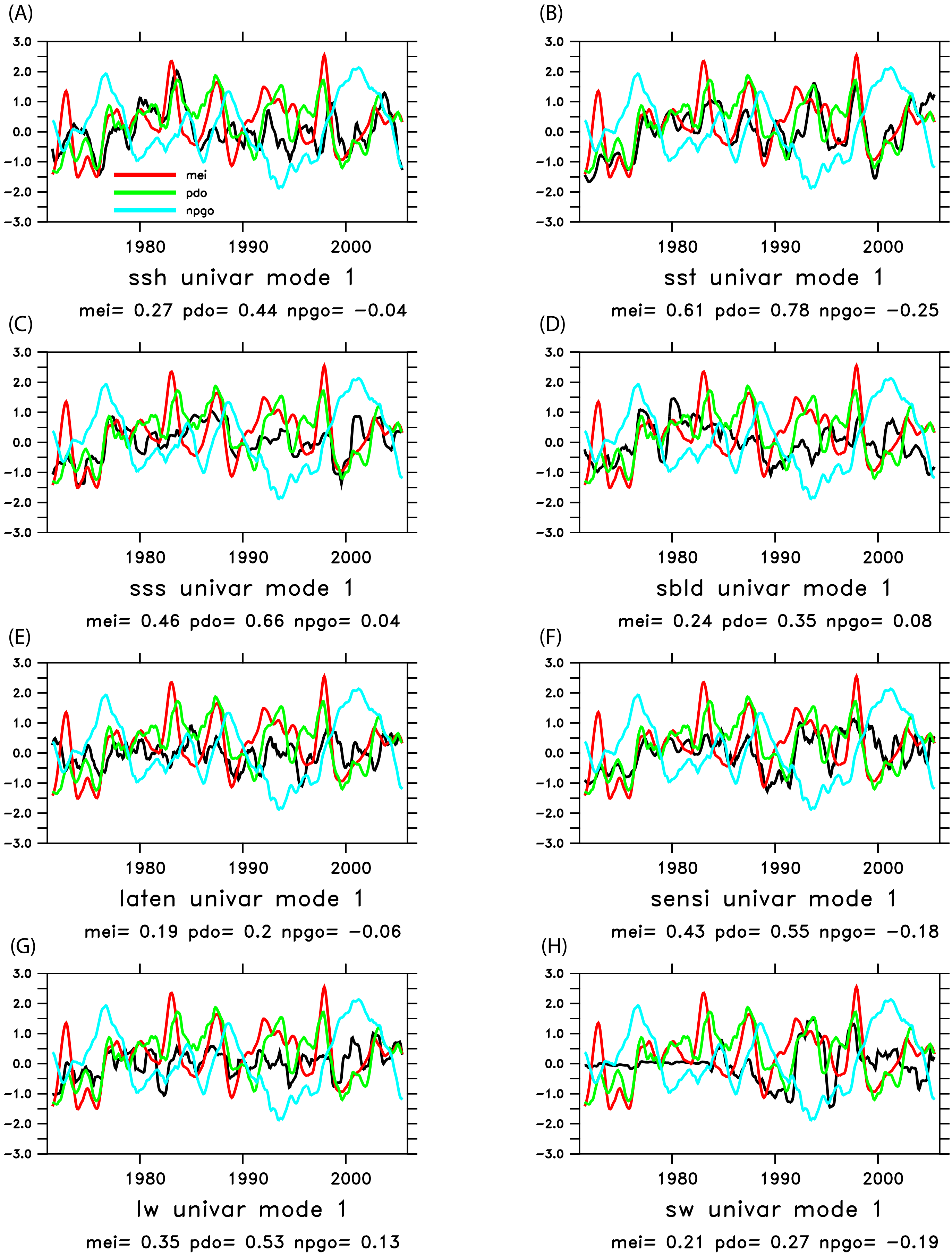
(A)
mei
pdo
npgo
ssh univar mode 1
mei= 0.27 pdo= 0.44 npgo= −0.04
(B)
sst univar mode 1
mei= 0.61 pdo= 0.78 npgo= −0.25
(C)
sss univar mode 1
mei= 0.46 pdo= 0.66 npgo= 0.04
(D)
sbld univar mode 1
mei= 0.24 pdo= 0.35 npgo= 0.08
(E)
laten univar mode 1
mei= 0.19 pdo= 0.2 npgo= −0.06
(F)
sensi univar mode 1
mei= 0.43 pdo= 0.55 npgo= −0.18
(G)
lw univar mode 1
mei= 0.35 pdo= 0.53 npgo= 0.13
(H)
sw univar mode 1
mei= 0.21 pdo= 0.27 npgo= −0.19

Figure 5

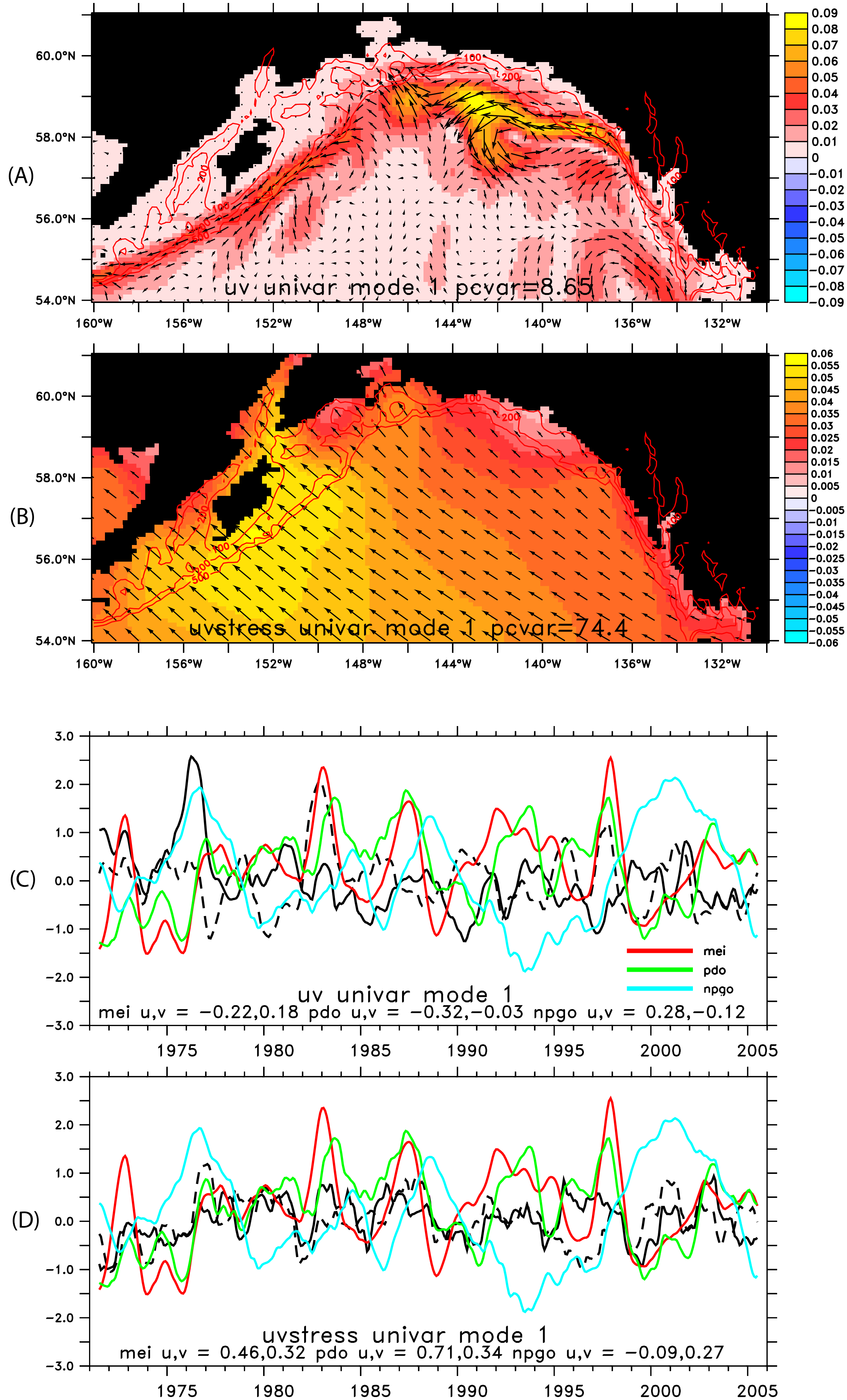
(A)
uv univar mode 1 pcvar=8.65
(B)
uvstress univar mode 1 pcvar=74.4
(C)
uv univar mode 1
mei u,v = −0.22,0.18 pdo u,v = −0.32,−0.03 npgo u,v = 0.28,−0.12
mei
pdo
npgo
(D)
uvstress univar mode 1
mei u,v = 0.46,0.32 pdo u,v = 0.71,0.34 npgo u,v = −0.09,0.27

Figure 6

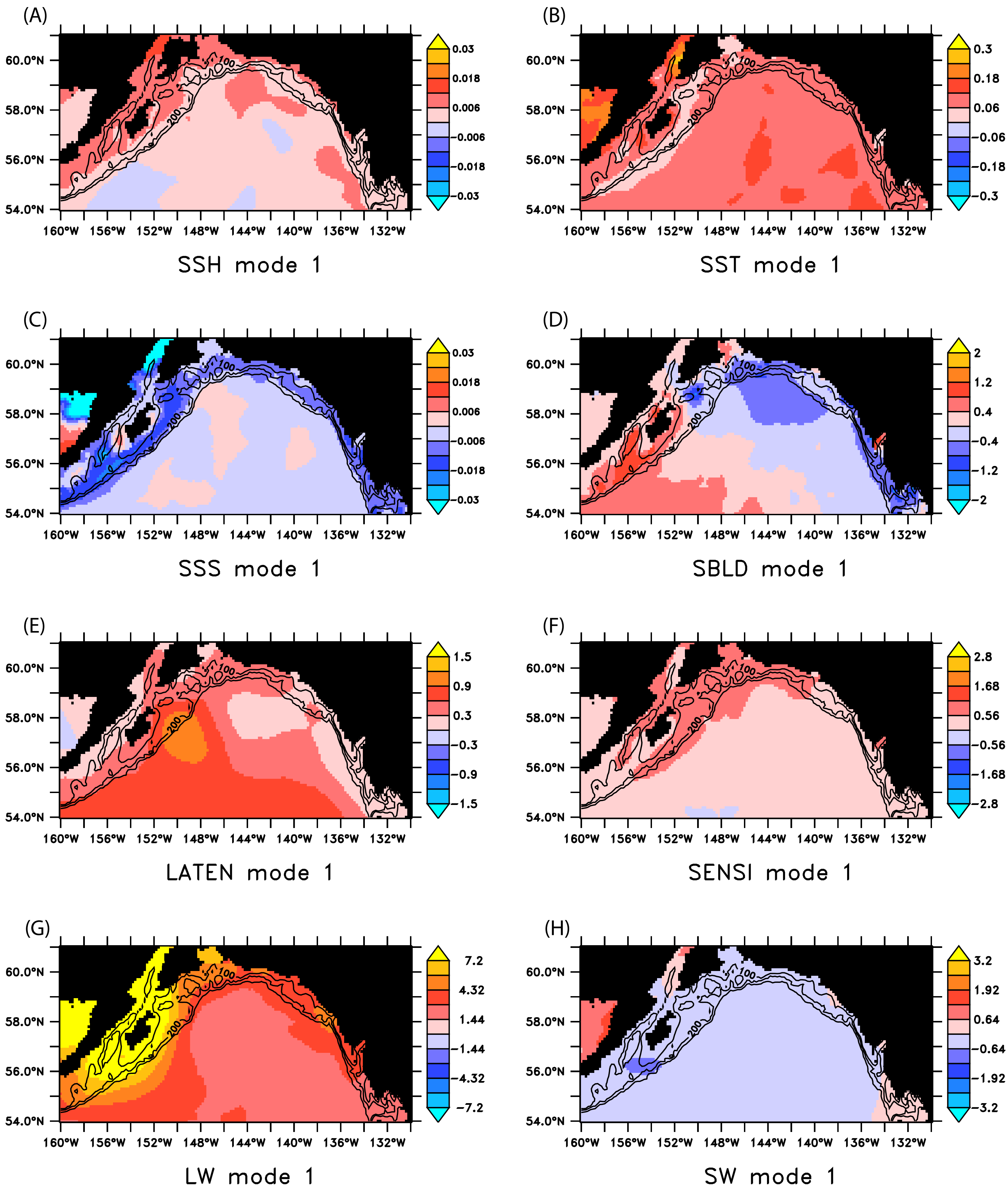
(A)
60.0°N
58.0°N
56.0°N
54.0°N
160°W 156°W 152°W 148°W 144°W 140°W 136°W 132°W
100
200
0.03
0.018
0.006
−0.006
−0.018
−0.03
SSH mode 1
(B)
0.3
0.18
0.06
−0.06
−0.18
−0.3
SST mode 1
(C)
0.03
0.018
0.006
−0.006
−0.018
−0.03
SSS mode 1
(D)
2
1.2
0.4
−0.4
−1.2
−2
SBLD mode 1
(E)
1.5
0.9
0.3
−0.3
−0.9
−1.5
LATEN mode 1
(F)
2.8
1.68
0.56
−0.56
−1.68
−2.8
SENSI mode 1
(G)
7.2
4.32
1.44
−1.44
−4.32
−7.2
LW mode 1
(H)
3.2
1.92
0.64
−0.64
−1.92
−3.2
SW mode 1

Figure 7

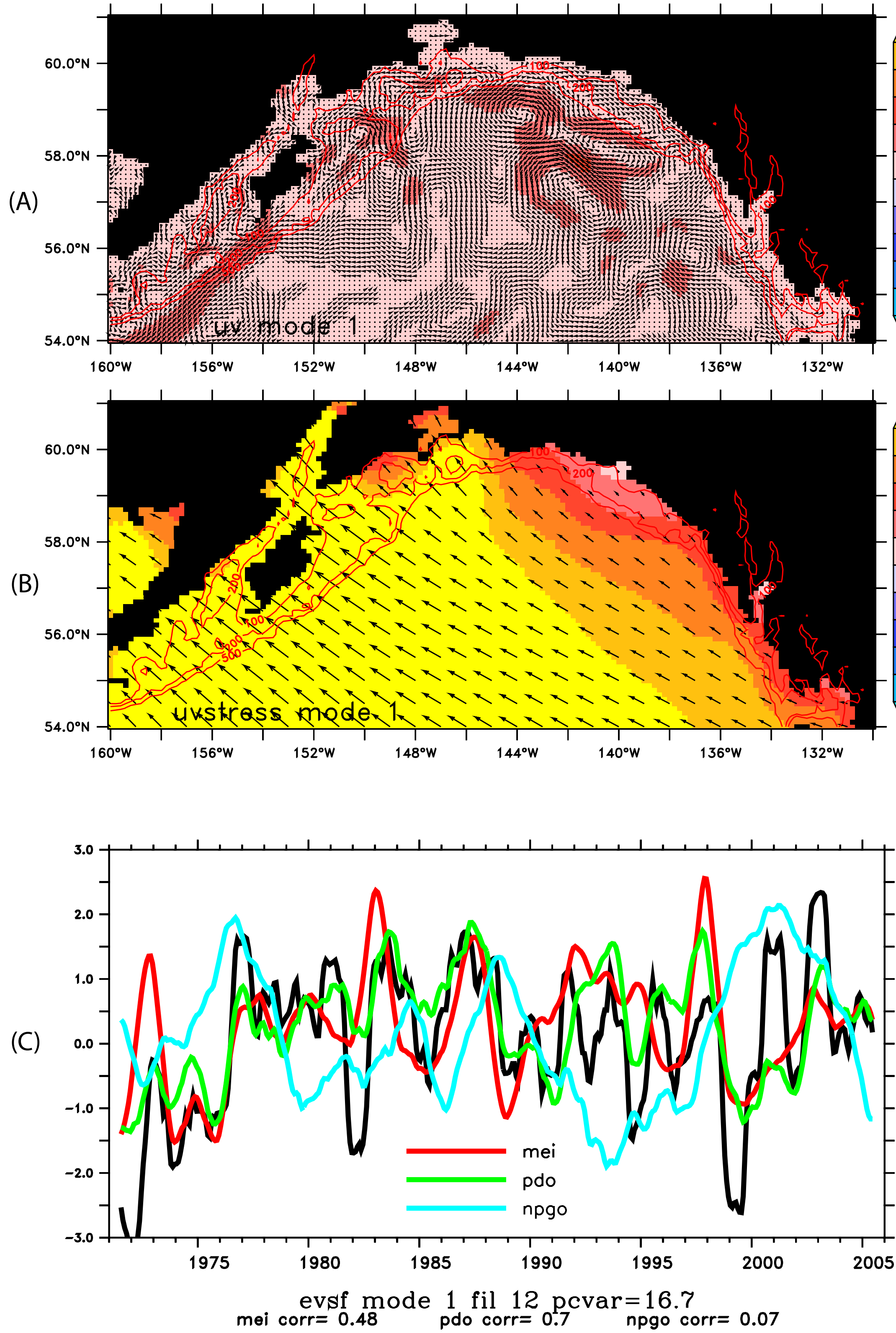
(A)
uv mode 1
60.0°N
58.0°N
56.0°N
54.0°N
160°W
156°W
152°W
148°W
144°W
140°W
136°W
132°W
0.02
0.016
0.012
0.008
0.004
0
-0.004
-0.008
-0.012
-0.016
-0.02
(B)
uvstress mode 1
0.01
0.008
0.006
0.004
0.002
0
-0.002
-0.004
-0.006
-0.008
-0.01
(C)
3.0
2.0
1.0
0.0
-1.0
-2.0
-3.0
1975
1980
1985
1990
1995
2000
2005
mei
pdo
npgo
evsf mode 1 fil 12 pcvar=16.7
mei corr= 0.48
pdo corr= 0.7
npgo corr= 0.07

Figure 8

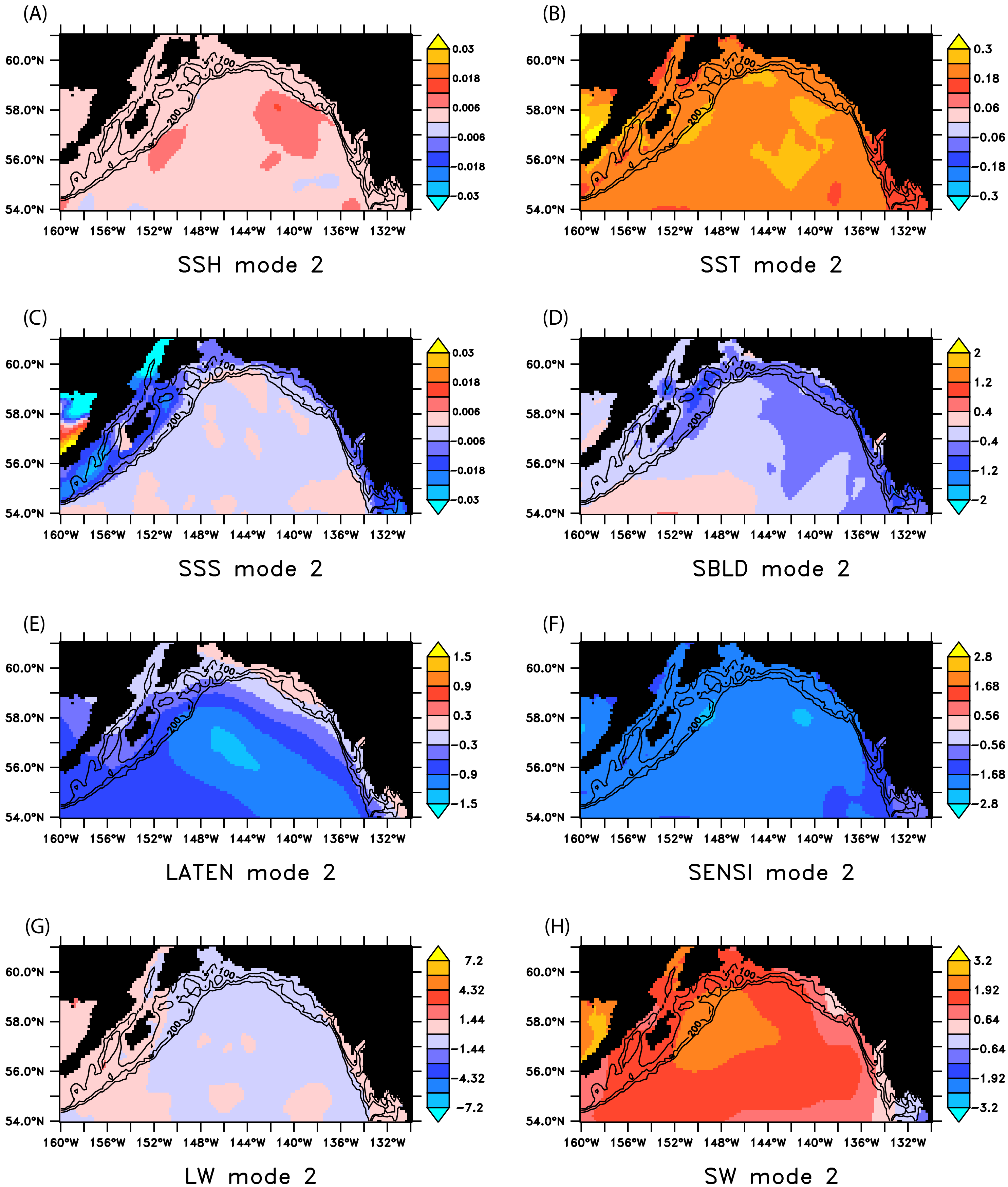

(A)
SSH mode 2
(B)
SST mode 2
(C)
SSS mode 2
(D)
SBLD mode 2
(E)
LATEN mode 2
(F)
SENSI mode 2
(G)
LW mode 2
(H)
SW mode 2

Figure 9

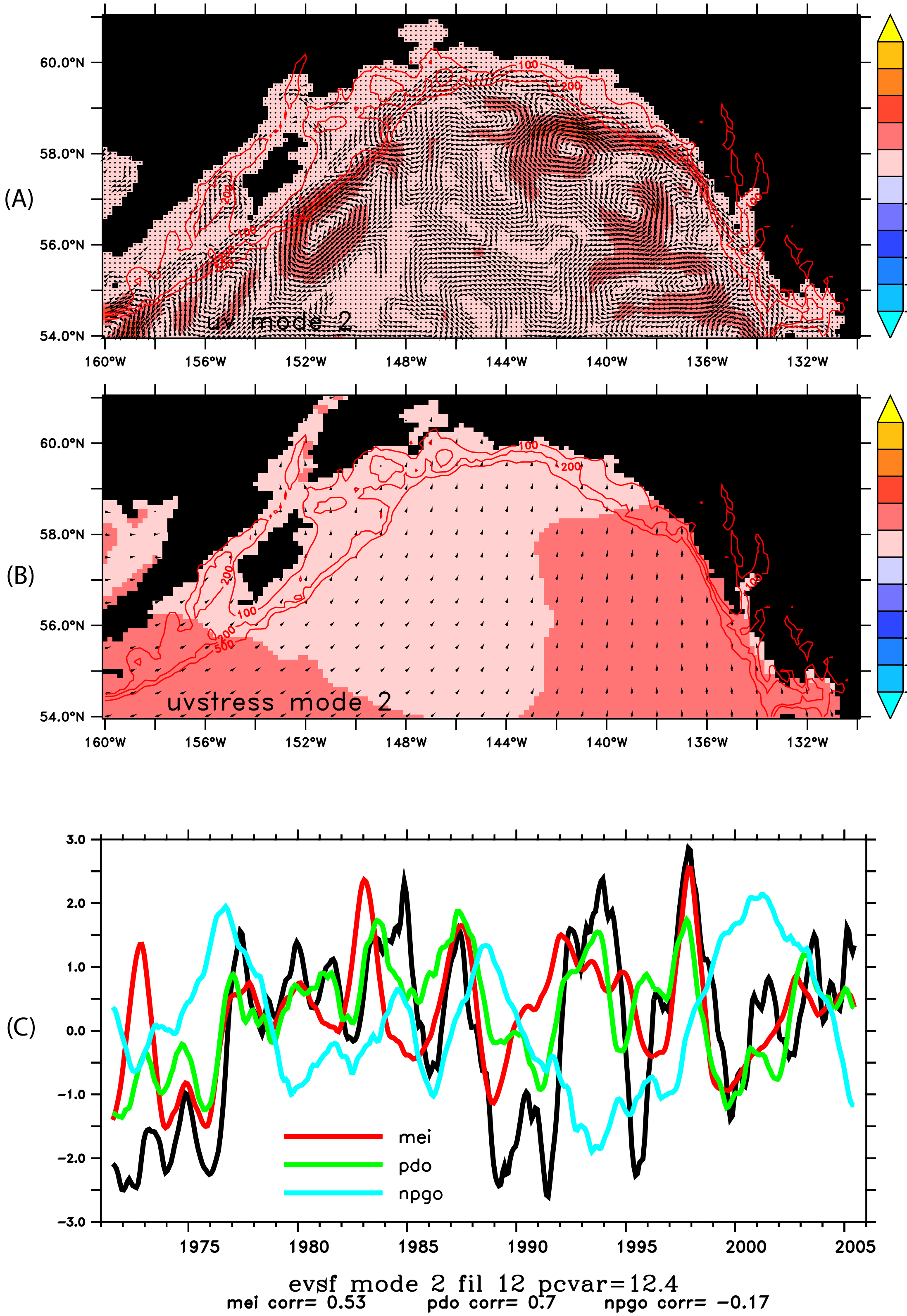
(A)
uv mode 2
(B)
uvstress mode 2
(C)
mei
pdo
npgo
evsf mode 2 fil 12 pcvar=12.4
mei corr= 0.53
pdo corr= 0.7
npgo corr= -0.17
60.0°N
58.0°N
56.0°N
54.0°N
160°W
156°W
152°W
148°W
144°W
140°W
136°W
132°W
1975
1980
1985
1990
1995
2000
2005

Figure 10

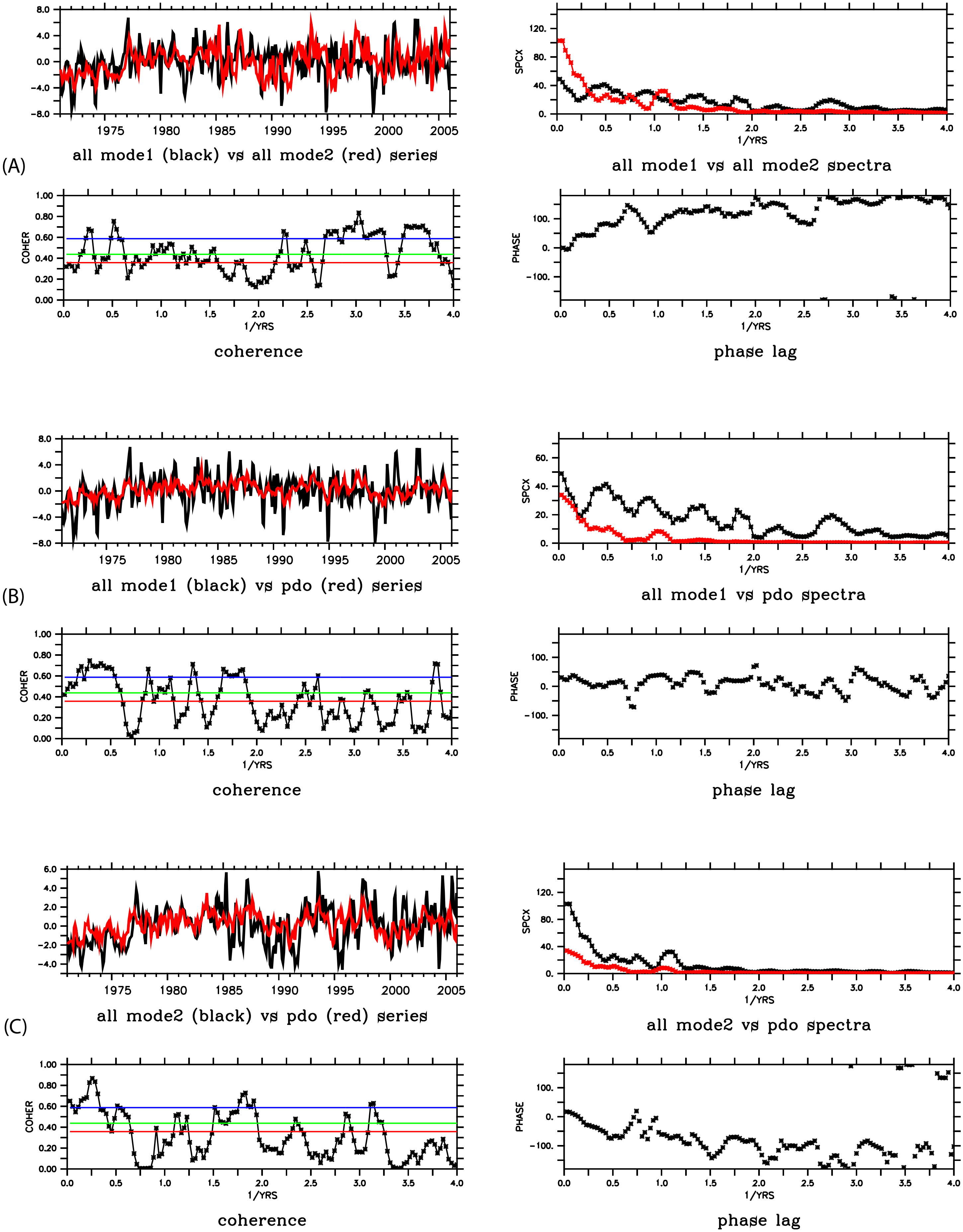
(A)
all mode1 (black) vs all mode2 (red) series
SPCX
1/YRS
all mode1 vs all mode2 spectra
COHER
1/YRS
coherence
PHASE
1/YRS
phase lag
(B)
all mode1 (black) vs pdo (red) series
SPCX
1/YRS
all mode1 vs pdo spectra
COHER
1/YRS
coherence
PHASE
1/YRS
phase lag
(C)
all mode2 (black) vs pdo (red) series
SPCX
1/YRS
all mode2 vs pdo spectra
COHER
1/YRS
coherence
PHASE
1/YRS
phase lag

Figure 11

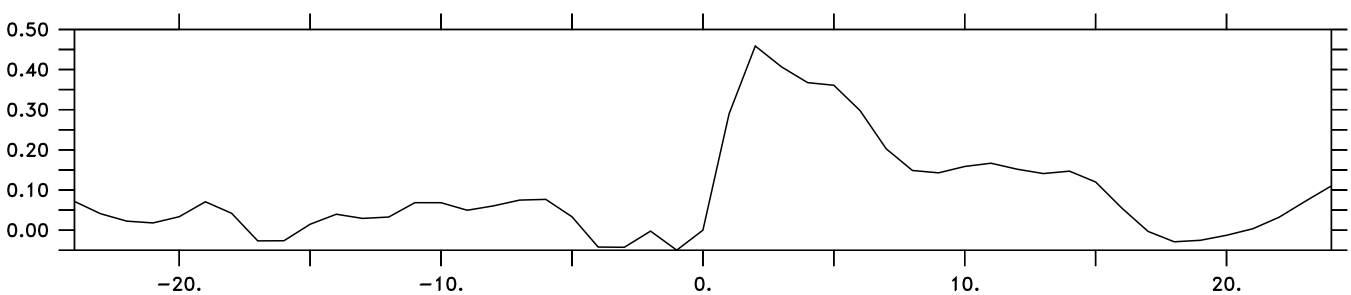

Figure 12

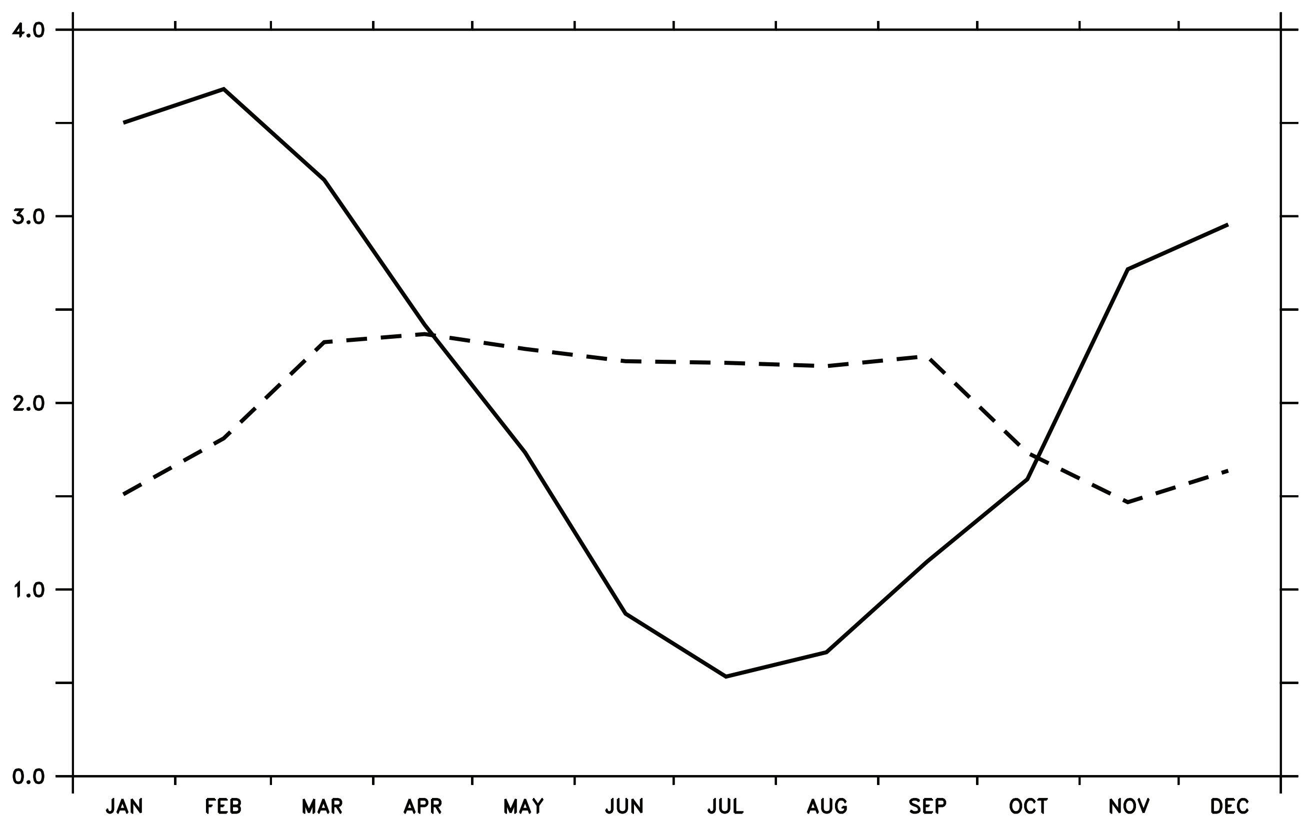

Figure 13

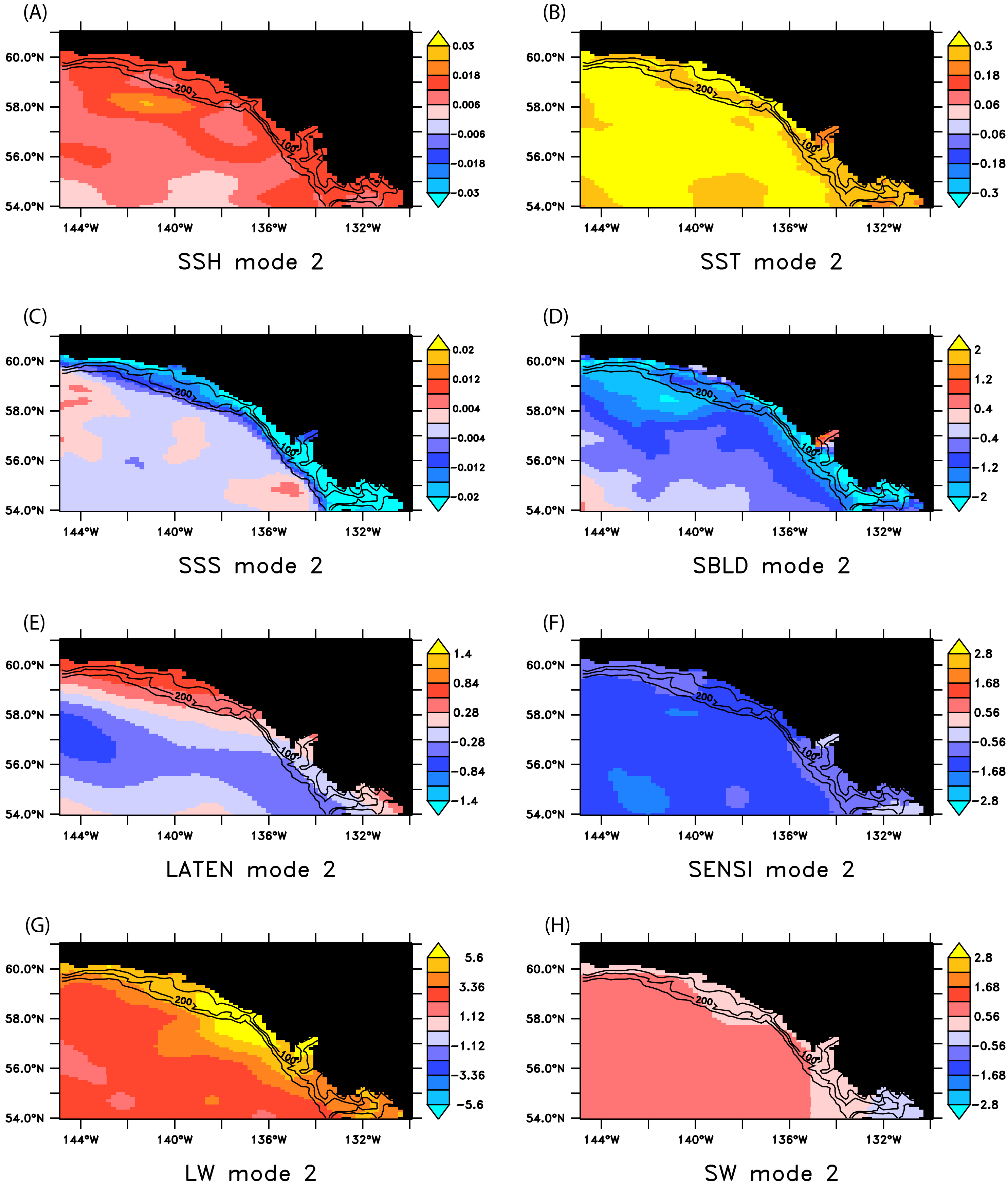
(A)
SSH mode 2
(B)
SST mode 2
(C)
SSS mode 2
(D)
SBLD mode 2
(E)
LATEN mode 2
(F)
SENSI mode 2
(G)
LW mode 2
(H)
SW mode 2

Figure 14

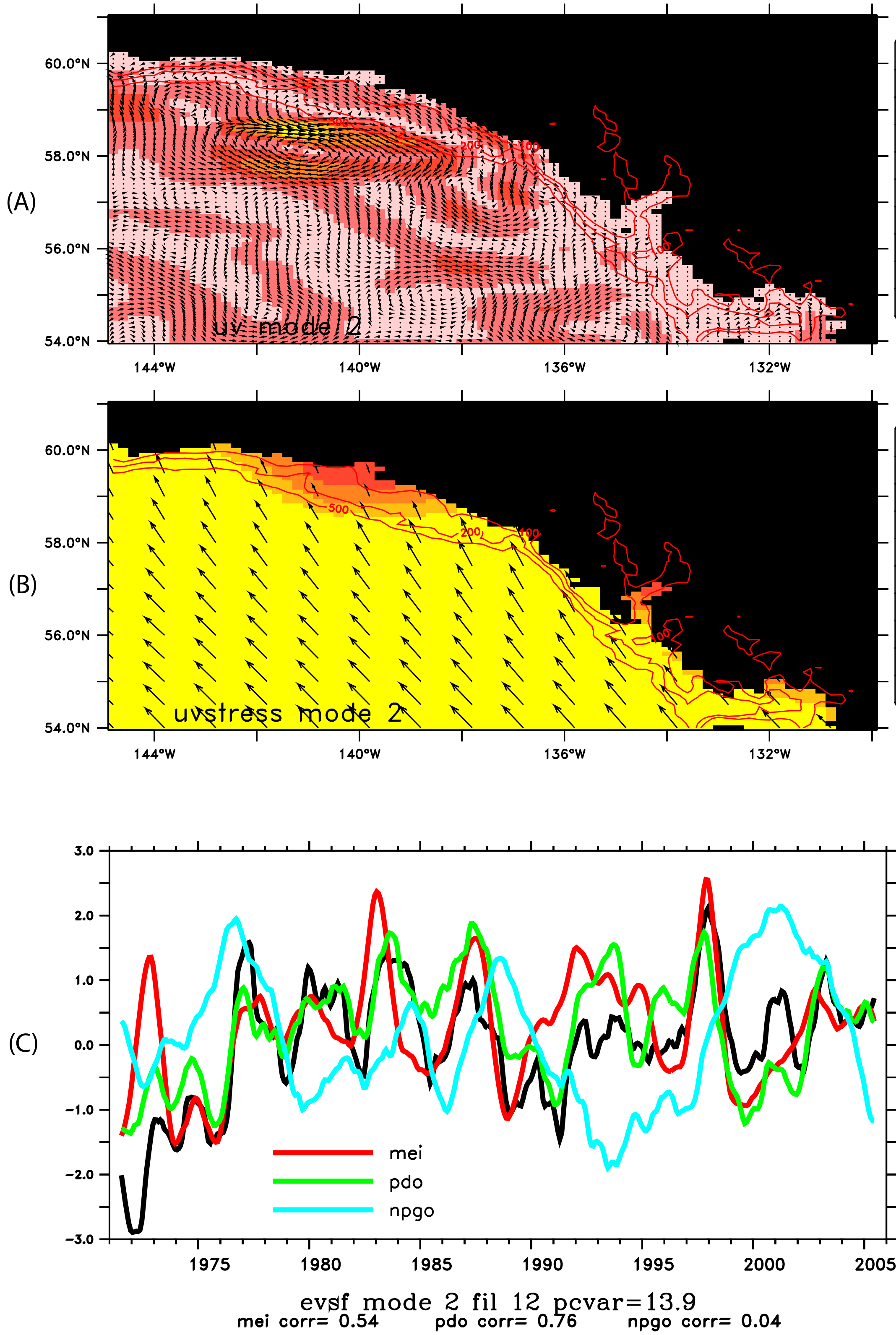
(A)
uv mode 2
60.0°N
58.0°N
56.0°N
54.0°N
144°W
140°W
136°W
132°W
0.02
0.016
0.012
0.008
0.004
0
-0.004
-0.008
-0.012
-0.016
-0.02
(B)
uvstress mode 2
500
200
100
0.01
0.008
0.006
0.004
0.002
0
-0.002
-0.004
-0.006
-0.008
-0.01
(C)
3.0
2.0
1.0
0.0
-1.0
-2.0
-3.0
1975
1980
1985
1990
1995
2000
2005
mei
pdo
npgo
evsf mode 2 fil 12 pcvar=13.9
mei corr= 0.54
pdo corr= 0.76
npgo corr= 0.04

Figure 15

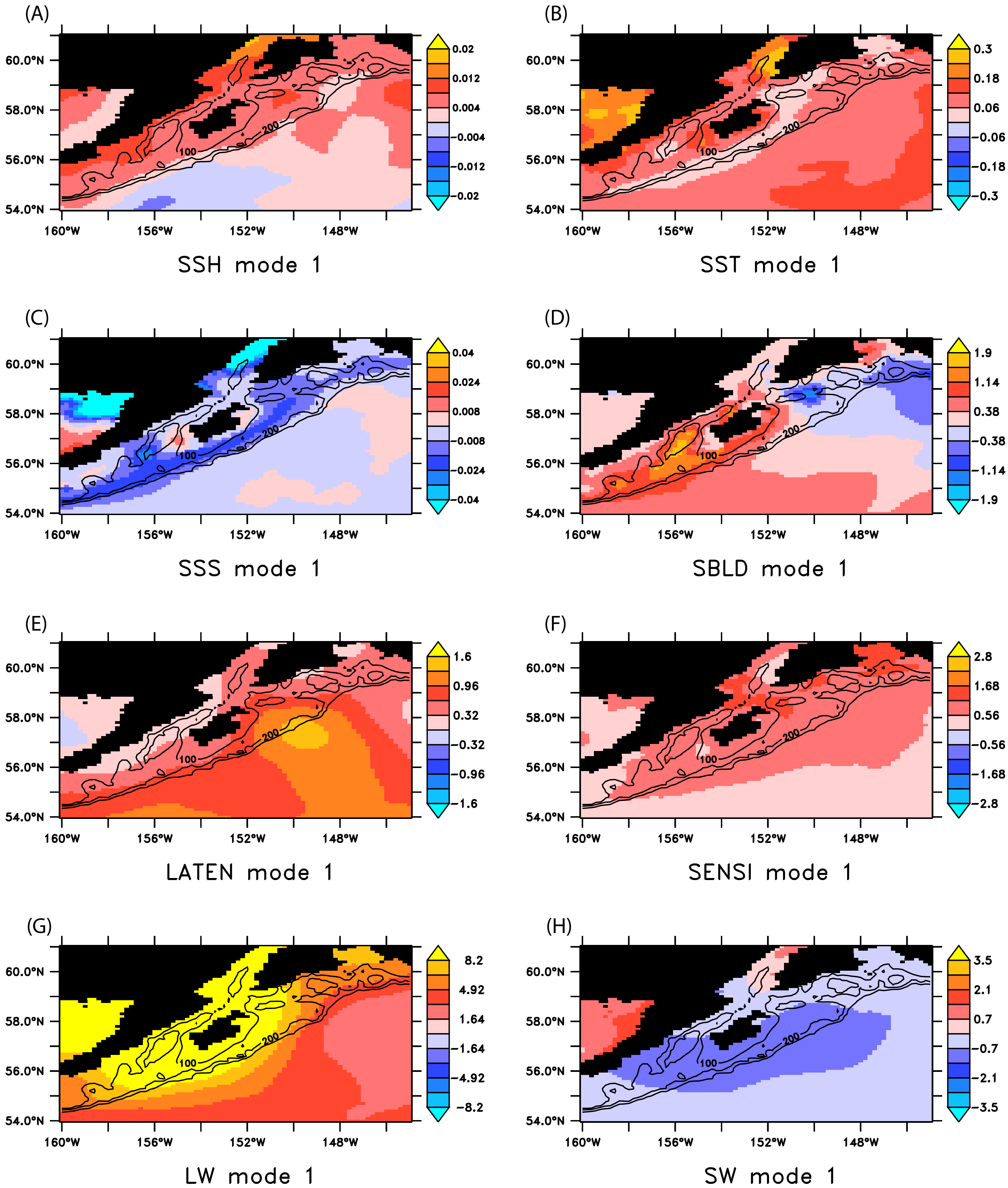
(A)
SSH mode 1
0.02
0.012
0.004
−0.004
−0.012
−0.02
(B)
SST mode 1
0.3
0.18
0.06
−0.06
−0.18
−0.3
(C)
SSS mode 1
0.04
0.024
0.008
−0.008
−0.024
−0.04
(D)
SBLD mode 1
1.9
1.14
0.38
−0.38
−1.14
−1.9
(E)
LATEN mode 1
1.6
0.96
0.32
−0.32
−0.96
−1.6
(F)
SENSI mode 1
2.8
1.68
0.56
−0.56
−1.68
−2.8
(G)
LW mode 1
8.2
4.92
1.64
−1.64
−4.92
−8.2
(H)
SW mode 1
3.5
2.1
0.7
−0.7
−2.1
−3.5
60.0°N
58.0°N
56.0°N
54.0°N
160°W
156°W
152°W
148°W
100
200

Figure 16

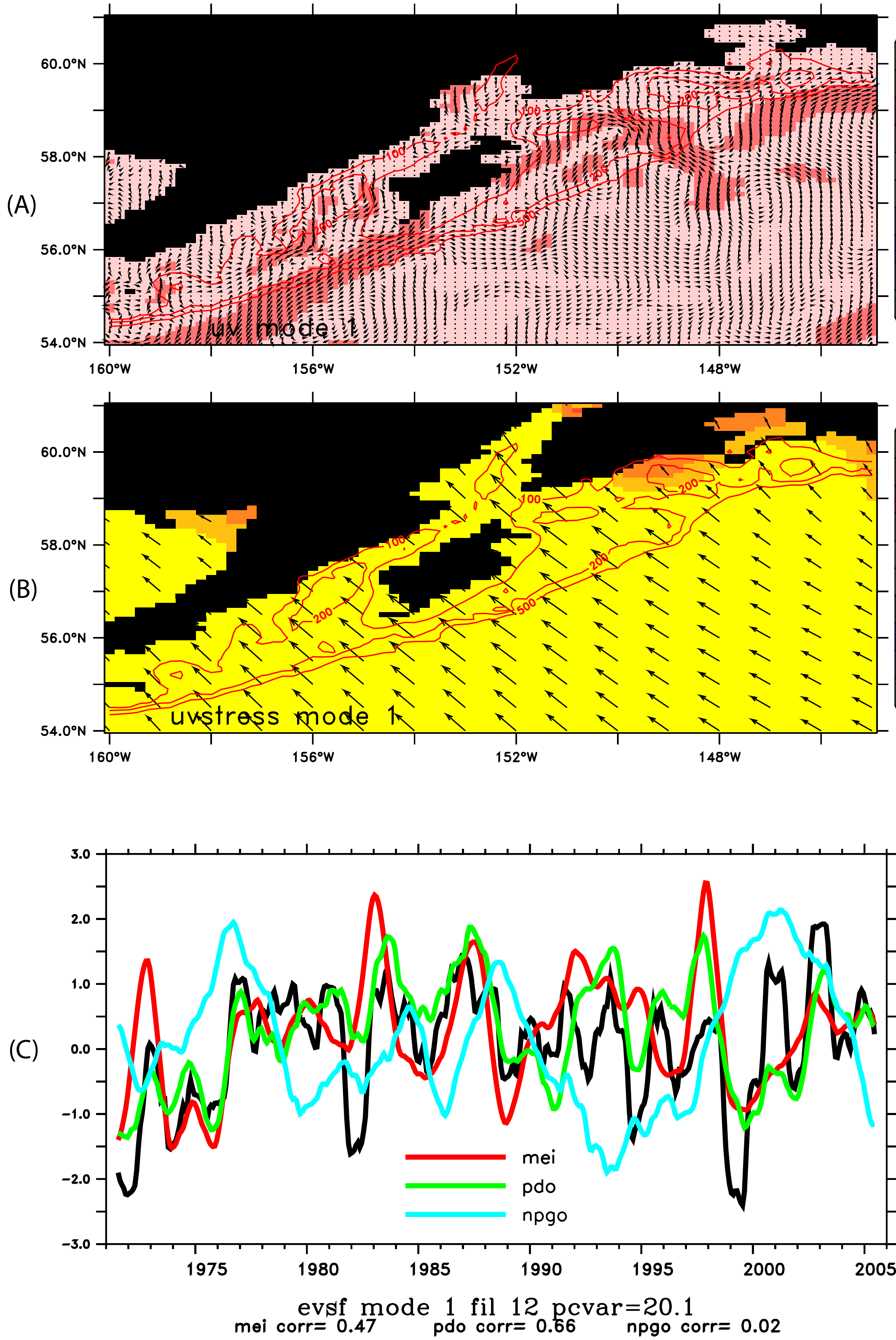
(A)
uv mode 1
60.0°N
58.0°N
56.0°N
54.0°N
160°W
156°W
152°W
148°W
0.02
0.016
0.012
0.008
0.004
0
−0.004
−0.008
−0.012
−0.016
−0.02
(B)
uvstress mode 1
0.01
0.008
0.006
0.004
0.002
0
−0.002
−0.004
−0.006
−0.008
−0.01
(C)
mei
pdo
npgo
evsf mode 1 fil 12 pcvar=20.1
mei corr= 0.47
pdo corr= 0.66
npgo corr= 0.02

Figure 17

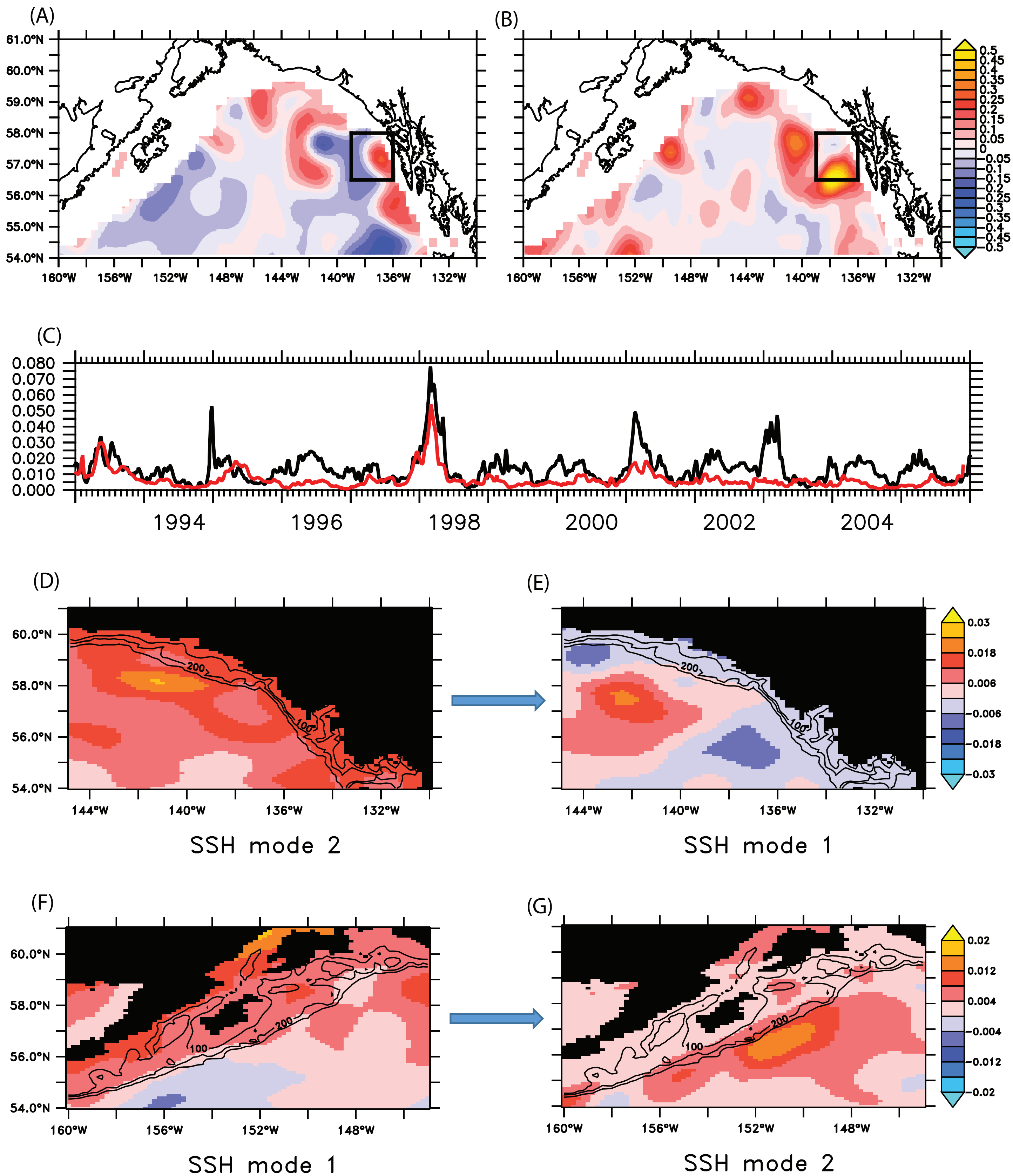
(A)
(B)
61.0°N
60.0°N
59.0°N
58.0°N
57.0°N
56.0°N
55.0°N
54.0°N
160°W
156°W
152°W
148°W
144°W
140°W
136°W
132°W
0.5
0.45
0.4
0.35
0.3
0.25
0.2
0.15
0.1
0.05
0
−0.05
−0.1
−0.15
−0.2
−0.25
−0.3
−0.35
−0.4
−0.45
−0.5
(C)
0.080
0.070
0.060
0.050
0.040
0.030
0.020
0.010
0.000
1994
1996
1998
2000
2002
2004
(D)
(E)
200
100
0.03
0.018
0.006
−0.006
−0.018
−0.03
SSH mode 2
SSH mode 1
(F)
(G)
0.02
0.012
0.004
−0.004
−0.012
−0.02
SSH mode 1
SSH mode 2

Figure 18